Technical Report

TR-2016-006

HiMod Reduction of Advection-Di usion-Reaction Problems with General Boundary Conditions

by

Matteo Aletti, Simona Perotto, Alessandro Veneziani

Mathematics and Computer Science

EMORY UNIVERSITY

Noname manuscript No.
(will be inserted by the editor)

HiMod Reduction of Advection-Diffusion-Reaction Problems with General Boundary Conditions

Matteo C. Aletti · Simona Perotto · Alessandro Veneziani

Received: date / Accepted: date

Abstract We extend the Hierarchical Model (HiMod) reduction procedure previously introduced in [11,24] to deal with general boundary conditions, enforcing their prescription in the basis function set. This is achieved by solving a Sturm-Liouville eigenvalue problem. We analyze this approach and provide a convergence analysis for the associated error in the case of a linear advection-diffusion-reaction problem in rectangles (2D) and slabs (3D). Numerical results confirm the theoretical investigation and the reliability of the proposed approach.

Keywords Model reduction · Spectral/Finite element combined approximation · Robin boundary conditions · Sturm-Liouville Eigenvalue problem

Mathematics Subject Classification (2000) 65N30 · 65N35 · 76M10 · 76M22 · 78M34

M.C. Aletti
Inria Paris & Sorbonne Universités UPMC Univ Paris 6,
Laboratoire Jacques-Louis Lions, France
E-mail: matteo.aletti@inria.fr

S. Perotto
MOX, Dipartimento di Matematica, Politecnico di Milano
P.zza L. da Vinci 32, I-20133 Milano, Italy
E-mail: simona.perotto@polimi.it

A. Veneziani
Department of Mathematics and Computer Science, Emory University
400 Dowman Dr NE, S.te N416, Atlanta GA, USA 30322
E-mail: ale@mathcs.emory.edu

1 Introduction

Efficient numerical solution of problems characterized by a main direction like flow in pipes and networks has been investigated in several ways, as witnessed by engineering and mathematical literature (see, e.g., [12,21,22]). A popular approach is based on reducing the problem of interest to a one-dimensional setting along the mainstream, after dropping transverse dynamics. The one-dimensional Euler equations in gas- and haemo-dynamics are a popular example. A different numerical approach known as Hierarchical Model (HiMod) reduction, yielding fast computation like for the one-dimensional models without discarding the transverse dynamics, has been proposed in [11,24], and successively investigated in [23,27,26,28]. In particular, the HiMod procedure follows the idea of combining separation of variables with a diverse numerical approximation, to take advantage from particular features of the problem at hand. Thus, along the mainstream we consider a classical one-dimensional finite element approximation to exploit easiness and versatility of this method. The transverse components are tackled by different approximations. In many applications of fluid dynamics, the cross-section of pipes is regular enough to accommodate a spectral approach [3,7–9,32–34]. The rapid convergence of spectral approximations allows to capture the important features of the transverse dynamics with a relatively low number of modes. This results in accurate approximations with a lower number of degrees of freedom in comparison with non-customized discretizations like classical finite elements. The separation of variables performed by a HiMod reduction carries several advantages also for the general structure of the algebraic problems, for model adaptivity [26] and for the efficiency of the solver. This has been recently demonstrated for the incompressible Navier-Stokes equations in biomedical applications in [14,19], both in terms of accuracy and computational efficiency.

One of the most significant limitations of the HiMod approach pursued so far is represented by the boundary conditions to prescribe on the lateral boundary of the domain. As a matter of fact, homogeneous Dirichlet conditions were promptly included by the basis functions adopted for this problem (either sinusoidal or polynomial). Although these conditions describe many practical applications, in view of generalizing the HiMod approach to more complex problems such as fluid-structure interaction, we need to address more general boundary conditions. We present here a possible method for this, which relies on the solution of an appropriate Sturm-Liouville eigenvalue problem [6]. This allows to design the modal basis to include, in an essential way, general boundary conditions and some features of the problem to solve, so that we call this an *educated basis*, while referring to the associated HiMod formulation as to *e-HiMod reduction*. Using the Sturm-Liouville eigenvalue problems in the HiMod setting represents the main novelty of this work.

The paper is organized as follows. Section 2 provides some hints to perform a HiMod reduction. In Section 3 we recall the basic properties for a Sturm-Liouville eigenvalue problem, and explicitly provide some proofs for general boundary conditions, the standard literature being essentially focused

on Dirichlet boundary data. In Section 4 we introduce the e-HiMod methodology in either two-dimensional rectangular domains or three-dimensional slabs, together with an *a priori* analysis of the associated model reduction error. Numerical results confirming theoretical findings are presented both in two-dimensional and three-dimensional domains in Section 5, dealing with linear advection-diffusion-reaction problems. A backward facing step geometry is finally used to test the e-HiMod procedure on a nontrivial slab-like domain. Limitations and future developments are summarized in Section 6.

2 The HiMod approach: basics

Since in this paper we are concerned with rectangular/slab domains, we directly assume that $\Omega \subset \mathbb{R}^d$ $(d = 2, 3)$ coincides with the Cartesian product $\Omega_{1D} \times \gamma$, where $\Omega_{1D} = [0, L]$ is the supporting domain and $\gamma = (0, 1)^{d-1}$ is the transverse fiber (see Figure 1). While this is the domain we will consider in presenting the method, it is important to stress that the entire procedure can be extended to more complex geometries. In the latter case, the domain considered here has the role of a reference geometry, as done, for instance, in a Dirichlet boundary condition setting in [19]. The space coordinates on γ will be denoted by $\mathbf{y}$. The axial direction associated with Ω_{1D} is dominant with respect to the others (i.e., $L \gg 1$). In general, we may assume Ω_{1D} to be a curve $\mathcal{C} : (0, L) \to \Omega_{1D} \subset \mathbb{R}^2$, where x denotes a curvilinear abscissa [23,25], while fiber γ is replaced by a fiber γ_x coinciding with a regular function of x.

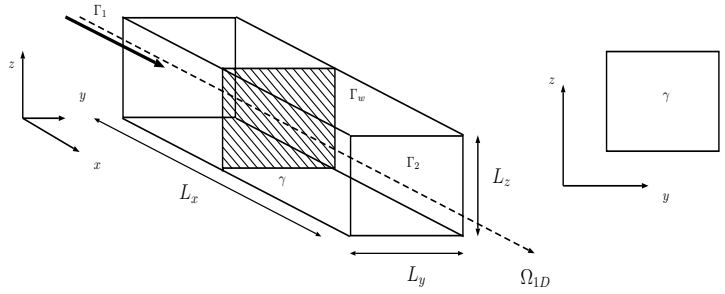

Fig. 1 3D slab domain Ω (left) and transverse fiber γ (right).

In Ω we solve the standard scalar linear advection-diffusion-reaction (ADR) problem completed with (homogeneous) generic boundary conditions,

$$\mathcal{L}u = f \quad \text{in } \Omega, \qquad \mathcal{B}u = 0 \quad \text{on } \partial\Omega, \tag{1}$$

where $\mathcal{L} : V \to V'$ stands for the differential operator $\mathcal{L}u = -\nabla \cdot (\mu \nabla u) + \nabla \cdot (\boldsymbol{\beta} u) + \sigma u$, from the Hilbert space $V \subset H^1(\Omega)$ (whose definition depends on the boundary conditions) to its dual V', and $\mathcal{B}u = 0$ denotes generically standard boundary conditions (Dirichlet, Neumann, Robin), possibly coexistent

on different portions of $\partial\Omega$. With standard arguments (and notation) [18], we associate with this problem the bilinear form $a(u,v)$ on $V \times V$ and the functional $F(v)$ with arguments in V, as follows

$$a(u,v) = \int_\Omega \left[\mu \nabla u \cdot \nabla v + \nabla \cdot \left(\boldsymbol{\beta} u\right) + \sigma u)v\right] d\Omega, \quad F(v) = \int_\Omega f v \, d\Omega. \tag{2}$$

We postulate the boundary $\partial\Omega$ to consist of the two transverse fibers $\Gamma_1 = \{0\} \times \gamma$ and $\Gamma_2 = \{L\} \times \gamma$, and of the lateral boundary $\Gamma_w = \partial\Omega \setminus \{\Gamma_1 \cup \Gamma_2\}$ (see Figure 1). The present paper focuses on the treatment of generic boundary conditions on Γ_w. For simplicity, we assume Dirichlet homogeneous data on Γ_1 and Γ_2. The extension to more general conditions on these portions of the boundary is straightforward and considered already in [24]. In addition, we assume the diffusivity coefficient $\mu \in L^\infty(\Omega)$, with $\mu \geq \mu_0 > 0$ a.e. in Ω, the convective field $\boldsymbol{\beta} \in [L^\infty(\Omega)]^d$, the reactive coefficient $\sigma \in L^\infty(\Omega)$, and the forcing term $f \in L^2(\Omega)$. We also assume that $\nabla \cdot \boldsymbol{\beta} \in L^\infty(\Omega)$ and that $-\frac{1}{2}\nabla \cdot \boldsymbol{\beta} + \sigma > 0$ a.e. in Ω, so that the bilinear form is *coercive* and the well-posedness of the weak form of (1) follows from the Lax-Milgram lemma. Correspondingly to the boundary conditions in (1), we denote by $V = H^1_*(\Omega)$ the subspace of $H^1(\Omega)$ functions such that $\mathcal{B}u = 0$ on $\partial\Omega$, the boundary conditions being imposed in an essential way, regardless of the specific type.

The HiMod formulation requires a specific function setting. We introduce the one-dimensional space $V_{1D} = H^1_0(\Omega_{1D})$ associated with the supporting fiber. On the transverse direction, we consider a set of modal functions $\{\varphi_k\}_k$, defined on γ such that $\mathcal{B}\varphi_k = 0$, and set

$$V_{\gamma,m} = \text{span}(\{\varphi_k\}_{k=1}^m).$$

Thus, the hierarchically reduced semi-discrete space is given by

$$V_m = \left\{ v(x,\mathbf{y}) = \sum_{k=1}^m v_k(x)\varphi_k(\mathbf{y}), \text{ with } v_k \in V_{1D} \text{ for } k = 1 \dots m \right\}. \tag{3}$$

We assume that $V_m \subset V$ for any $m \in \mathbb{N}$ (*conformity hypothesis*), and that, for any $v \in V$, $\lim_{m\to+\infty} \left(\inf_{v_m \in V_m} ||v - v_m||_V\right) = 0$ (*spectral approximability hypothesis*). When we let m tend to infinity, we identify the space V_∞. The conformity and spectral approximability properties postulated on V_m imply that V_∞ is dense in V.

The basis functions $\{\varphi_k\}_k$ do not need to be generally orthonormal. However, if we assume they are orthonormal with respect to the $L^2(\gamma)$-scalar product, $(\cdot,\cdot)_\gamma$, the coefficients v_k in (3) coincide with the standard Fourier coefficients $v_k = (v, \varphi_k)_\gamma$. Modal functions $\{\varphi_k\}_k$ can be selected a priori, being, for instance, trigonometric functions, Legendre polynomials or B-splines [5,14,11, 19,24,23,25]. In this work, we investigate a new method, where the differential operator $\mathcal{L}$ drives this choice.

The fully-discrete HiMod formulation is obtained by introducing a uniform subdivision $\mathcal{T}_h$ of step h along Ω_{1D}, with the nodes x_i, $i = 0, 1, \dots, N_h$.

The generalization to the case of non-uniform adapted partitions is considered in [26]. Let V^h be the subspace of V_{1D} of the continuous piecewise linear functions associated with $\mathcal{T}_h$ and vanishing at $x_0 = 0$ and $x_{N_h} = L$. Higher order discretizations can be considered as well [25]. Correspondingly, we define the space V_m^h of functions in the form $\sum_{k=1}^{m} v_k^h(x)\varphi_k(\mathbf{y})$, with $v_k^h(x) \in V^h$. Let ψ_i denote the Lagrangian basis function in V^h associated with the node x_i. Thus, we can consider the discrete modal representation

$$u_m^h(x,\mathbf{y}) = \sum_{k=1}^{m} u_k^h(x)\varphi_k(\mathbf{y}) = \sum_{k=1}^{m}\sum_{i=1}^{N_h} u_{k,i}\psi_i(x)\varphi_k(\mathbf{y}), \tag{4}$$

where $u_{k,i}$ are the actual unknowns of the discrete HiMod formulation

$$\text{find } u_m^h \in V_m^h : a(u_m^h, v_m^h) = F(v_m^h) \quad \forall v_m^h \in V_m^h, \tag{5}$$

with $u_k^h(x) = \sum_{i=1}^{N_h} u_{k,i}\psi_i(x) \in V^h$. A natural choice for the test function in (5) is $v_m^h(x,\mathbf{y}) = \psi_l(x)\varphi_j(\mathbf{y})$, with $l = 1,\dots,N_h$, $j = 1,\dots,m$. Then, the HiMod formulation (5) reduces to: find $u_{k,i} \in \mathbb{R}$, with $k = 1,\dots,m$ and $i = 1,\dots,N_h$, such that, for any $j = 1,\dots,m$ and for any $l = 1,\dots,N_h$,

$$\sum_{k=1}^{m}\sum_{i=1}^{N_h}\Big\{\int_{\Omega_{1D}}\Big[\; r_{k,j}^{11}(x)\frac{\partial\psi_i}{\partial x}(x)\frac{\partial\psi_l}{\partial x}(x) + r_{k,j}^{10}(x)\frac{\partial\psi_i}{\partial x}(x)\psi_l(x) + \; r_{k,j}^{00}\psi_i(x)\psi_l(x)\Big]\,dx\Big\}u_{k,i} = \int_{\Omega_{1D}}\psi_l(x)f_j(x)\,dx. \tag{6}$$

Following [11], in the case of homogeneous Dirichlet data also on Γ_w, coefficients $r_{k,j}^{st}$, with $s,t = 0,1$, and f_j are given by

$$\begin{aligned}
&r_{k,j}^{11}(x) = \int_\gamma \mu(x,\mathbf{y})\varphi_j(\mathbf{y})\varphi_k(\mathbf{y})\,d\mathbf{y}, \quad r_{k,j}^{10}(x) = \int_\gamma \beta_1(x,\mathbf{y})\varphi_j(\mathbf{y})\varphi_k(\mathbf{y})\,d\mathbf{y},\\
&r_{k,j}^{00}(x) = \int_\gamma \Big(\mu(x,\mathbf{y})\varphi_j'(\mathbf{y})\varphi_k'(\mathbf{y}) + \beta_2(x,\mathbf{y})\varphi_j'(\mathbf{y})\varphi_k(\mathbf{y}) + \sigma(x,\mathbf{y})\varphi_j(\mathbf{y})\varphi_k(\mathbf{y})\Big)d\mathbf{y},\\
&f_j(x) = \int_\gamma f(x,\mathbf{y})\varphi_j(\mathbf{y})\,d\mathbf{y},
\end{aligned} \tag{7}$$

respectively, where φ_l' denotes the derivative of the generic modal function φ_l with respect to $\mathbf{y}$. In particular, coefficients $r_{k,j}^{st}$ $(s,t = 0,1)$ account for the transverse dynamics after the reduction phase. From an algebraic viewpoint, discretization (6) leads to a system of m coupled one-dimensional problems, characterized by a block tridiagonal sparsity pattern.

The convergence of the HiMod discrete solution u_m^h to the continuous one u for $m \to +\infty$ and $h \to 0$ is stated in Proposition 3.1 of [24] when Dirichlet boundary conditions are assigned on Γ_w. For instance, in Figure 2 we show the

results of a test case on a slab, carried out with the open source library `LifeV`[1]. Specifically, we provide the results of a constant coefficient ADR problem characterized by a forcing term featuring two Gaussian functions centered at two distinct points. Homogeneous Dirichlet conditions are prescribed on Γ_w and Γ_1, while homogeneous Neumann data are assigned on Γ_2. Visual inspection of the contour plots highlights the agreement of the HiMod approximation with the finite element solution, progressively improving with m. The finite element solution is obtained with a piecewise linear approximation on a uniform grid ($h_x = 0.1$, $h_y = h_z = h_x/2$). The HiMod approximation is yielded on the same one-dimensional grid along the x-axis and with an increasing number of modes. For $m = 25$ the agreement between the two solutions is excellent. Figure 3 highlights how the HiMod solution is consistently more accurate with respect to the full 3D finite element approximation for a fixed number of degrees freedom (left panel), and requires a much faster assembly for a desired error (right panel). More details on this test case can be found in [1]. These excellent results in the presence of lateral homogeneous Dirichlet boundary conditions motivate the search of a general strategy to deal with all the possible boundary data.

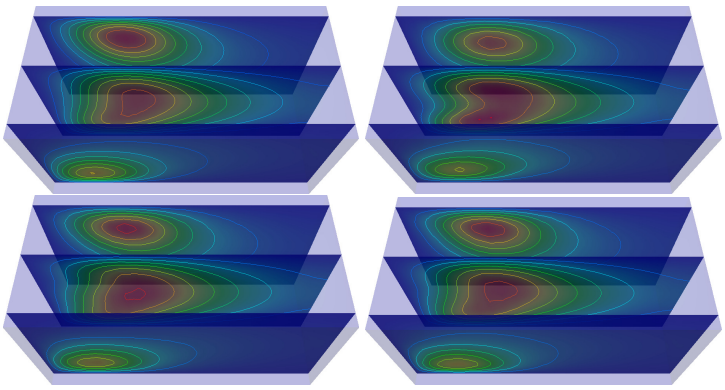

Fig. 2 3D ADR problem: longitudinal sections of the FE solution (top-left) and of the HiMod solutions for $m = 9$ (top-right), $m = 16$ (bottom-left) and $m = 25$ (bottom-right).

3 The Sturm-Liouville Eigenvalue (SLE) problem in the HiMod framework

Directional model reduction has been considered in different contexts. In particular, in [32] the reduction is oriented to shell structure problems and the

[1] `LifeV` is an open source finite element library developed by MOX at Politecnico di Milano, Italy, the Department of Mathematics at EPFL, Switzerland and the Department of Mathematics and Computer Science at Emory University, USA [17].

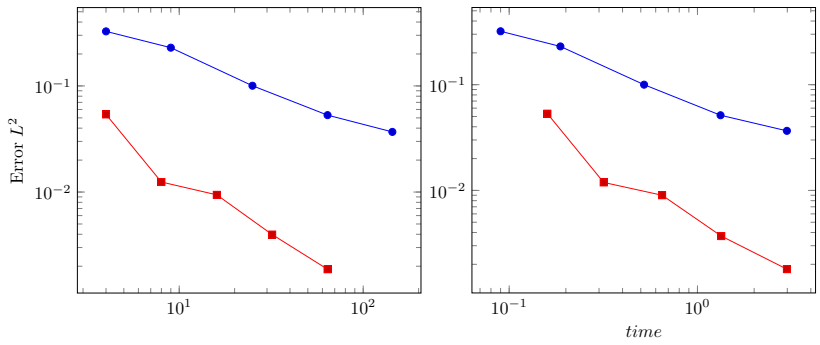

Fig. 3 3D ADR problem with lateral Dirichlet boundary conditions: $L^2(\Omega)$-norm of the global error as a function of the number of dof (left) and of the assembly time [s] (right) for a standard 3D linear finite element discretization (circle markers) and for a HiMod approximation (square markers).

optimal selection of the reduced basis is functional to the small size of the transverse dimension. In the present work we are not interested in analyzing the modeling error as a function of the transverse size of the domain. We construct our discussion purely on the spectral approximation properties of the basis functions. The choice of the modal basis can be done in several ways for Dirichlet boundary conditions [11,24,19,20], yet the case of general conditions needs to be carefully addressed.

The construction of the modal basis here relies on the eigenfunctions of an appropriate differential operator designed on the problem to solve. In particular, when considering the template problem (1), we search a basis function set incorporating the lateral boundary conditions in an essential way.
Let $\mathcal{L}_S : V \to L^2(\Omega)$ be the symmetric part of the ADR operator,

$$\mathcal{L}_S u = -\nabla \cdot (\mu \nabla u) + \widetilde{\sigma} u, \tag{8}$$

with $\widetilde{\sigma} = \sigma + \frac{1}{2}\nabla \cdot \boldsymbol{\beta}$. Since there is no ambiguity in what follows, we adopt the same symbol to denote the restriction of this operator to the $d-1$-dimensional fiber γ. Then, the computation of a HiMod basis for problem (1) is obtained by solving the eigenvalue problem

$$\mathcal{L}_S \varphi = \lambda \varphi \quad \text{in } \gamma, \qquad \mathcal{B}\varphi = 0 \quad \text{on } \partial\gamma. \tag{9}$$

We postulate the problem coefficients to be regular enough for the operator $\mathcal{L}_S$ to be self-adjoint. Problem (9) is a classical Sturm Liouville Eigenvalue (SLE) problem, largely investigated in the literature of partial differential equations as a natural tool for analytically solving simple problems by separation of variables/superposition of effects [5,6,29]. We recall here the basic properties of SLE problems and provide proofs in a general context, as many references are mostly concerned with one-dimensional problems completed with Dirichlet boundary conditions.

3.1 Spectrum of a self-adjoint elliptic operator

We consider the SLE problem with the general form

$$\mathcal{L}_S\varphi_k(\mathbf{y}) = \lambda_k w(\mathbf{y})\varphi_k(\mathbf{y}) \quad \text{in } \gamma, \qquad \mathcal{B}\varphi_k(\mathbf{y}) = 0 \quad \text{on } \partial\gamma, \tag{10}$$

where λ_k is the eigenvalue of $\mathcal{L}_S$ associated with the eigenfunction φ_k, while the weight w is a positive continuous function. The following statements hold:

1. the eigenvalues $\{\lambda_k\}_k$ are real and form a countable monotone non-decreasing sequence convergent to infinity for $k \to +\infty$. In the one-dimensional case, the multiplicity of every eigenvalue is equal to one (it may be greater for singular SLE problems, where μ is allowed to vanish on the boundary);
2. the eigenfunctions $\{\varphi_k\}_k$ are orthonormal with respect to the scalar product of the weighted space $L^2_w(\gamma)$. They constitute a complete set in the same space. This means that, for a generic function $f \in L^2_w(\gamma)$, the truncated series
$$\mathcal{S}_m f(\mathbf{y}) = \sum_{k=1}^{m} \hat{f}_k \varphi_k(\mathbf{y}), \tag{11}$$
with $\hat{f}_k = \displaystyle\int_\gamma w(\mathbf{y}) f(\mathbf{y})\varphi_k(\mathbf{y})\, d\mathbf{y}$, is such that $\lim_{m\to+\infty} \|f - \mathcal{S}_m f\|_w = 0$, with $\|\cdot\|_\omega$ the norm associated with the space $L^2_w(\gamma)$. From now on, we refer to the basis functions $\{\varphi_k\}_k$ in (10) guaranteeing expansion (11) as to the SL basis;
3. for $k \to +\infty$, the eigenvalues in (10) are such that
$$\lambda_k \sim \mathcal{O}\left(\frac{k^{\frac{2}{d-1}}}{|\gamma|}\right), \tag{12}$$
with $|\gamma|$ the size of the fiber γ. Result (12) follows from the so-called Weyl formula [35, 29].

3.2 Approximability properties

Let $\mathcal{R}_m f$ denote the *residual* associated with the m-th truncated series (11), namely

$$\mathcal{R}_m f(\mathbf{y}) = f(\mathbf{y}) - \mathcal{S}_m f(\mathbf{y}) = \sum_{k=m+1}^{+\infty} \hat{f}_k \varphi_k(\mathbf{y}).$$

We will investigate the convergence rate of the residual with respect to m on the domain γ. To this aim, we first establish the dependence of the generalized Fourier coefficient $\hat{f}_k$ on the eigenvalue λ_k. In particular, when function f belongs at least to $H^2(\gamma)$, we can compute also the generalized Fourier series of $\mathcal{L}_S f$, whose k-th coefficient will be denoted by $\widehat{\mathcal{L}_S f}_k$.

Lemma 1 *Let φ_k be the eigenfunction solution to problem* (10)*, and let $f \in H^2(\gamma)$ be a generic function fulfilling the same boundary conditions as φ_k. Then,*

$$\hat{f}_k = \frac{1}{\lambda_k}\widehat{\mathcal{L}_S f}_k \quad \forall k \geq 1. \tag{13}$$

Moreover, if $f \in H^{2p}(\gamma)$, with $p \geq 2$, and $\mathcal{L}_S^r f$ satisfies the same boundary conditions as f for any $r \leq p-1$ (i.e., $\mathcal{L}_S^r f$ satisfies what we refer to as compatible boundary conditions up to order $p-1$*), then*

$$\hat{f}_k = \left(\frac{1}{\lambda_k}\right)^p \widehat{\mathcal{L}_S^p f}_k \quad \forall k \geq 1, \tag{14}$$

where $\widehat{\mathcal{L}_S^p f}_k$ denotes the k-th coefficient of the generalized Fourier series associated with the p-th power of the operator $\mathcal{L}_S$.

Proof Statement (13) follows from (10) and from the fact that $\mathcal{L}_S$ is a self-adjoint operator in $L^2_w(\gamma)$, so that,

$$\hat{f}_k = (f, \varphi_k)_{L^2_w(\gamma)} = \frac{1}{\lambda_k}(f, \mathcal{L}_S\varphi_k)_{L^2_w(\gamma)} = \frac{1}{\lambda_k}(\mathcal{L}_S f, \varphi_k)_{L^2_w(\gamma)} = \frac{1}{\lambda_k}\widehat{\mathcal{L}_S f}_k. \tag{15}$$

Now, if we consider a function $f \in H^{2p}(\gamma)$ for some $p \geq 2$ and such that $\mathcal{L}_S^r f$ fulfills the same boundary conditions as f for $r \leq p-1$, we can iterate the same argument as in (15), to obtain

$$\widehat{\mathcal{L}_S^r f}_k = \frac{1}{\lambda_k}\widehat{\mathcal{L}_S^{r+1} f}_k. \tag{16}$$

By properly combining (15) with (16), we obtain (14).

□

From now on, for simplicity, we set $w = 1$, as this is the only case we actually considered in the numerical assessment. The convergence of $\mathcal{R}_m f$ as a function of m is stated in the following result.

Theorem 1 *Let φ_k be the eigenfunction, solution to problem* (10)*, and let $f \in H^2(\gamma)$ satisfy the same boundary conditions as φ_k. Then, there exists a constant $C_{1,s}$ independent of m, such that*

$$||\mathcal{R}_m f||_{H^s(\gamma)} \leq C_{1,s}\left(\frac{1}{m+1}\right)^{\frac{2-s}{d-1}} \|f\|_{H^2(\gamma)},$$

for $s = 0, 1$, and with $H^0(\gamma) = L^2(\gamma)$. Moreover, if $f \in H^{2p}(\gamma)$, with $p \geq 2$, and $\mathcal{L}_S^r f$ satisfies compatible boundary conditions up to order $p-1$, then there exists a constant $C_{2,s}$, independent of m, such that, for $s = 0, 1$,

$$||\mathcal{R}_m f||_{H^s(\gamma)} \leq C_{2,s}\left(\frac{1}{m+1}\right)^{\frac{2p-s}{d-1}} \|f\|_{H^{2p}(\gamma)}. \tag{17}$$

Proof We first consider the case $s = 0$. By resorting to Parseval's identity, we have

$$||\mathcal{R}_m f||^2_{L^2(\gamma)} = \sum_{k=m+1}^{+\infty} \hat{f}_k^2.$$

The properties of the SLE problem listed above together with relation (13) guarantee that the right-hand side converges to zero for $k \to \infty$. In addition, the slowest term to converge is the one associated with $k = m + 1$ since coefficients $\hat{f}_k$ inversely depend on λ_k. Thanks to Lemma 1, formula (12) and the $L^2(\gamma)$-orthonormality of functions $\{\varphi_k\}_k$, we have that, if $f \in H^2(\gamma)$ and satisfies the same boundary conditions as φ_k, then

$$||\mathcal{R}_m f||^2_{L^2(\gamma)} \leq \Big(\frac{1}{\lambda_{m+1}}\Big)^2 \sum_{k=m+1}^{+\infty} \big[\widehat{\mathcal{L}_S f}_k\big]^2 \leq \frac{C}{(m+1)^{\frac{4}{d-1}}} \|f\|^2_{H^2(\gamma)}, \qquad (18)$$

with C depending on $|\gamma|$ and on the problem data, μ, $\boldsymbol{\beta}$ and σ. Analogously, if $f \in H^{2p}(\gamma)$ for some $p \geq 2$, and $\mathcal{L}_S^r f$ satisfies the same boundary conditions as f for any $r \leq p - 1$, we have

$$||\mathcal{R}_m f||^2_{L^2(\gamma)} \leq \Big(\frac{1}{\lambda_{m+1}}\Big)^{2p} \sum_{k=m+1}^{+\infty} \big[\widehat{\mathcal{L}_S^p f}_k\big]^2 \leq \frac{C}{(m+1)^{\frac{4p}{d-1}}} \|f\|^2_{H^{2p}(\gamma)}. \qquad (19)$$

Now, we select $s = 1$. With the operator $\mathcal{L}_S$, we associate the symmetric, continuous and coercive bilinear form

$$a_S(\varphi_k, v) = \int_\gamma \big[\mu \nabla \varphi_k \cdot \nabla v + \widetilde{\sigma} \varphi_k v\big]\, d\gamma,$$

defined in $V_\gamma = H^1_*(\gamma)$ the subspace of $H^1(\gamma)$ functions satisfying the assigned boundary conditions in an essential way. This form induces the scalar product $\big((w, v)\big) = a_S(w, v)$ for any w, $v \in V_\gamma$, and the associated norm $\|w\|^2_{a_S} = a_S(w, w)$ for any $w \in V_\gamma$. In particular, the functions $\left\{\widetilde{\varphi}_k = \frac{\varphi_k}{\sqrt{\lambda_k}}\right\}_k$ form an orthonormal basis in $H^1(\gamma)$ with respect to the scalar product $\big((\cdot, \cdot)\big)$ [31]. The *generalized* Fourier coefficients $\widetilde{f}_k$ of f with respect to this basis are related to the coefficients in (11) simply by integration by parts, since

$$\widetilde{f}_k = \big((f, \widetilde{\varphi}_k)\big) = a_S(f, \widetilde{\varphi}_k) = \lambda_k(f, \widetilde{\varphi}_k) = \sqrt{\lambda_k}(f, \varphi_k) = \sqrt{\lambda_k}\, \hat{f}_k.$$

Via Parseval's identity and thanks to the coercivity of the bilinear form $a_S(\cdot, \cdot)$, we obtain

$$\alpha_S \|\mathcal{R}_m f\|^2_{H^1(\gamma)} \leq ||\mathcal{R}_m f||^2_{a_S} = \sum_{k=m+1}^{+\infty} \widetilde{f}_k^2 = \sum_{k=m+1}^{+\infty} \lambda_k \hat{f}_k^2,$$

with α_S the coercivity constant associated with $a_S(\cdot, \cdot)$. The same arguments adopted in (18) and (19) lead to the estimate

$$||\mathcal{R}_m f||^2_{H^1(\gamma)} \leq \frac{\alpha_S^{-1}}{\lambda_{m+1}} \sum_{k=m+1}^{+\infty} \big[\widehat{\mathcal{L}_S f}_k\big]^2 \leq \frac{C}{(m+1)^{\frac{2}{d-1}}} \|f\|^2_{H^2(\gamma)},$$

and

$$||\mathcal{R}_m f||^2_{H^1(\gamma)} \leq \alpha_S^{-1}\Big(\frac{1}{\lambda_{m+1}}\Big)^{2p-1} \sum_{k=m+1}^{+\infty} \big[\widehat{\mathcal{L}_S^p f}_k\big]^2 \leq \frac{C}{(m+1)^{\frac{4p-2}{d-1}}} \|f\|^2_{H^{2p}(\gamma)},$$

respectively, where C now depends also on the coercivity constant α_S. This concludes the proof.

□

Remark 1 For $p \to \infty$, estimate (17) yields spectral convergence. In the specific case of Neumann conditions, this means that an infinitely regular function f with all the odd derivatives vanishing at the boundary is spectrally approximated by generalized Fourier truncated series. This result is recalled, for instance, in Section 2.2 of [6] with no proof.

3.2.1 The case of Neumann boundary conditions

Driven by numerical evidence, for the case with Neumann boundary conditions (and still with a self-adjoint coercive operator $\mathcal{L}_S$), we can prove an additional result under some regularity assumptions that, however, do not involve the boundary conditions for the derivatives of f (as opposed to Theorem 1). At the best of authors' knowledge, this result is non standard.

In what follows, we assume the coefficients μ, $\boldsymbol{\beta}$ and σ in (8) to be regular enough to make each step formally correct.

Lemma 2 *Let φ_k be the eigenfunction, solution to problem* (10) *completed with homogeneous Neumann boundary conditions. If $f \in H^4(\gamma)$ and satisfies homogeneous Neumann boundary conditions as φ_k, then we have*

$$|\hat{f}_k| \leq C\frac{1}{\lambda_k^{3/2}}\|f\|_{H^4(\gamma)} \quad \forall k \geq 1, \tag{20}$$

with $C = C(\tau)$, τ being the constant associated with the trace inequality. In addition, if the basis functions $\{\varphi_k\}_k$ are uniformly bounded with respect to k, then the previous statement improves into

$$|\hat{f}_k| \leq C\frac{1}{\lambda_k^{2}}\|f\|_{H^4(\gamma)} \quad \forall k \geq 1. \tag{21}$$

Remark 2 The requirement of uniform boundedness is satisfied by several functions, such as Legendre polynomials, sinusoidal or Bessel functions (for Bessel functions, we refer to [15]). These functions represent standard choices for the modal basis in a HiMod reduction [24, 19, 14].

For the sake of brevity, we give the proof of Lemma 2 together with the proof of the following result.

Theorem 2 *Let φ_k be the eigenfunction, solution to problem* (10) *completed with homogeneous Neumann boundary conditions. If $f \in H^4(\gamma)$ and satisfies homogeneous Neumann boundary conditions as φ_k, then there exists a constant $C_{3,s}$, independent of m, such that, for $s = 0, 1$,*

$$||\mathcal{R}_m f||_{H^s(\gamma)} \leq C_{3,s} \left(\frac{1}{m+1}\right)^{\frac{3-s}{d-1}} ||f||_{H^4(\gamma)}. \tag{22}$$

In addition, if the basis functions $\{\varphi_k\}_k$ are uniformly bounded with respect to k, then there exists a constant $C_{4,s}$, independent of m, such that

$$|\mathcal{R}_m f||_{H^s(\gamma)} \leq C_{4,s} \left(\frac{1}{m+1}\right)^{\frac{4-s}{d-1}} ||f||_{H^4(\gamma)}. \tag{23}$$

Proof If $f \in H^4(\gamma)$, it is possible to mimic the procedure adopted in Lemma 1, by working directly on the coefficients of the generalized Fourier series for $\mathcal{L}_S f$. However, we can improve the previous estimates by explicitly exploiting the Neumann boundary conditions. Via integration by parts and thanks to (10), we have

$$\begin{aligned}
\widehat{\mathcal{L}_S f}_k &= -\int_\gamma \nabla \cdot (\mu \nabla f)\, \varphi_k \, d\mathbf{y} + \int_\gamma \widetilde{\sigma} f \varphi_k d\mathbf{y} \\
&= \frac{1}{\lambda_k} \left[\int_\gamma \nabla \cdot (\mu \nabla f)\, \nabla \cdot (\mu \nabla \varphi_k)\, d\mathbf{y} - \int_\gamma \widetilde{\sigma} \nabla \cdot (\mu \nabla f)\, \varphi_k d\mathbf{y} \right. \\
&\quad \left. - \int_\gamma \widetilde{\sigma} \nabla \cdot (\mu \nabla \varphi_k)\, f d\mathbf{y} + \int_\gamma \widetilde{\sigma}^2 f \varphi_k d\mathbf{y} \right] \\
&= \frac{1}{\lambda_k} \left[\int_\gamma \nabla \cdot (\mu \nabla (\nabla \cdot (\mu \nabla f)))\, \varphi_k d\mathbf{y} - \int_\gamma \widetilde{\sigma} \nabla \cdot (\mu \nabla f)\, \varphi_k d\mathbf{y} \right. \\
&\quad - \int_\gamma \nabla \cdot (\mu \nabla (\widetilde{\sigma} f))\, \varphi_k d\mathbf{y} + \int_\gamma \widetilde{\sigma}^2 f \varphi_k d\mathbf{y} \\
&\quad \left. - \int_{\partial\gamma} \nabla (\nabla \cdot (\mu \nabla f)) \cdot \mathbf{n}\, \mu \varphi_k ds + \int_{\partial\gamma} \nabla (\widetilde{\sigma} f) \cdot \mathbf{n}\, \mu \varphi_k ds \right].
\end{aligned} \tag{24}$$

Thus, by combining (15) with (24), and by exploiting the trace inequality together with the $L^2(\gamma)$-orthonormality of functions $\{\varphi_k\}_k$, we obtain the relation

$$|\hat{f}_k| \leq C \frac{1 + \tau^2 \|\varphi_k\|_{H^1(\gamma)}}{\lambda_k^2} \|f\|_{H^4(\gamma)} \tag{25}$$

with C a constant depending on the problem data and τ the constant of the trace inequality. In addition, since from the $L^2(\gamma)$-orthonormality of the eigenfunctions follows that $\|\varphi_k\|_{H^1(\gamma)} \simeq \sqrt{\lambda_k}$, we obtain (20). From (25), if $\{\varphi_k\}_k$ are uniformly bounded with k, then (21) follows.

Estimates (22) and (23) are an immediate consequence of (20) and (21) when we apply the arguments used in Theorem 1.

4 e-HiMod reduction

The ultimate goal of the procedure proposed in this paper is to construct an "educated" lifting for the boundary conditions imposed on the lateral surface of Ω. To this aim, we exploit the theory in the previous section and build a basis $\{\varphi_k\}_k$ which efficiently includes condition $\mathcal{B}u = 0$ on Γ_w in an essential way. We refer to such a basis as to an *educated basis* and we denote the corresponding hierarchical model reduction by *e-HiMod* approach.

The basic e-HiMod procedure consists of the following steps:

1. split the problem along the axial (one-dimensional) and the transverse direction, respectively;
2. solve the $(d-1)$-dimensional SLE problem (10) associated with the symmetric part $\mathcal{L}_S$ of the ADR operator on the transverse fiber γ, to obtain the modal basis $\{\varphi_k\}$;
3. assemble the HiMod block tridiagonal matrix associated with the one-dimensional mainstream coupled problems (6);
4. solve the HiMod system.

Some remarks are in order. Designing the SLE problem associated with the operator $\mathcal{L}$ by selecting the symmetric part $\mathcal{L}_S$ of $\mathcal{L}$ intends to be effective for model reduction, as we speculate that more the modal basis knows about the problem and fewer modes are required. Nevertheless, in the search of a trade-off between accuracy and efficiency, this may be practically sub-optimal, for instance in the presence of space dependent problem data or of unsteady problems with time-dependent data (a case out of the scope of the present work but undoubtedly critical in the follow up of the present research). Indeed, in the first case, problem (10) needs to be solved at each finite element node along the axial coordinate, whereas in an unsteady setting the SLE problem has to be recomputed at each time step. For the sake of computational efficiency, it is worth giving up the resemblance of the SLE self-adjoint operator to the ADR problem, in favour of a template constant-coefficient symmetric problem to solve once and for all. Thus, operator $\mathcal{L}_S$ is, in practice, designed by averaging the problem coefficients so to resort to elementary problems with, in most of the cases, an analytical solution (or where the numerical approximation is limited to the root-finding of the eigenvalues). For this reason, when focusing on step 2., we assume μ, $\boldsymbol{\beta}$ and σ in (2) to be constant. However, we stress that, by no means, this implies we can solve only problems with constant coefficients, as shown in Section 5. We argue that this choice results overall in the need of more modes to capture discrete dynamics with a given accuracy, yet with a global computational advantage.

Finally, we remark that, when $\Omega \subset \mathbb{R}^3$ (i.e., γ is a two-dimensional fiber), problem (10) can be furtherly split into the tensor product of one-dimensional problems, as we will detail in Section 4.2.

Now, we exemplify the e-HiMod reduction procedure on a two-dimensional and on a three-dimensional counterpart of problem (1).

4.1 2D e-HiMod reduction in rectangular domains

We complete problem (1) by prescribing the homogeneous Robin condition $\mu\nabla u \cdot \mathbf{n} + \chi u = 0$ on Γ_w, being $\Omega = (0, L) \times (0, 1)$ and by selecting constant problem data according to what observed in the previous section. First, we re-write the weak form of the problem by including the Robin condition as: find $u = u(x, y) \in V = H^1_{\Gamma_1 \cup \Gamma_2}(\Omega)$ such that

$$\begin{aligned}
&\int_0^L \int_0^1 \mu\Big(\frac{\partial u}{\partial x}(x,y)\frac{\partial v}{\partial x}(x,y) + \frac{\partial u}{\partial y}(x,y)\frac{\partial v}{\partial y}(x,y)\Big)dxdy + \int_0^L \chi u(x,1)v(x,1)dx \\
+ &\int_0^L \chi u(x,0)v(x,0)dx + \int_0^L \int_0^1 \Big(\beta_1 \frac{\partial u}{\partial x}(x,y)v(x,y) + \beta_2 \frac{\partial u}{\partial y}(x,y)v(x,y)\Big)dxdy \\
+ &\int_0^L \int_0^1 \sigma u(x,y)v(x,y)dxdy = \int_0^L \int_0^1 f(x,y)v(x,y)dxdy \quad \forall v \in V.
\end{aligned}$$

Now, we solve the SLE problem (10) with $w = 1$ to generate the educated modal basis $\{\varphi_k\}_{k=1}^m$ characterizing the HiMod approximation (4). The $L^2(\gamma)$-orthonormality of the eigenfunctions $\{\varphi_k\}_k$ simplifies the first two HiMod coefficients in (7) to

$$r^{11}_{k,j}(x) = \mu\delta_{jk}, \qquad r^{10}_{k,j}(x) = \beta_1\delta_{jk},$$

respectively. The third HiMod coefficient reduces to

$$r^{00}_{k,j}(x) = \int_0^1 \beta_2 \varphi_j'(y)\varphi_k(y)dy + \lambda_j\delta_{jk}$$

since, by exploiting problem (10) and the $L^2(\gamma)$-orthonormality of functions $\{\varphi_k\}_k$, it holds

$$\begin{aligned}
&\int_0^1 \Big(\mu\varphi_j'(y)\varphi_k'(y) + \sigma\varphi_j(y)\varphi_k(y)\Big)dy - \mu\Big[\varphi_j'(y)\varphi_k\Big]_0^1 \\
= &\int_0^1 \Big(\mu\varphi_j'(y)\varphi_k'(y) + \sigma\varphi_j(y)\varphi_k(y)\Big)dy + \chi[\varphi_j\varphi_k]_0^1 = \int_0^1 \lambda_j\varphi_j(y)\varphi_k(y)dy = \lambda_j\delta_{jk}.
\end{aligned}$$

Exploiting this circumstance, the assembly cost of the HiMod matrix significantly reduces when resorting to an educated basis, at least in the case of constant problem data. In addition, in the absence of a vertical convection (i.e., for $\beta_2 = 0$), the sparsity pattern becomes block-diagonal. This generally leads to a significant cost reduction for the linear algebra, as we have already noticed in Figure 3.

Remark 3 Non-homogeneous boundary conditions can be treated with appropriate lifting functions, for instance, via a modal expansion of the boundary data. In addition, the case where different types of boundary conditions are prescribed on different portions of Γ_w can be considered as well by a domain decomposition approach.

Remark 4 In many cases, the solution to the one-dimensional SLE problem (10) can be obtained analytically or after the numerical root-finding of a nonlinear function [5]. For instance, for the mixed homogeneous boundary conditions $\varphi_k(0) = 0$ and $\varphi_k'(1) + \chi\varphi_k(1) = 0$, the eigenvalues of problem (10) coincide with the roots of the nonlinear equation $\chi\tan(\lambda_k) + \lambda_k = 0$, while the eigenfunctions are given by $\varphi_k(y) = \sin(\lambda_k y)$, so that we deal with basis functions which are uniformly bounded with k (we also refer to Remark 7 for some additional considerations).

4.2 3D e-HiMod reduction in slab domains

We hierarchically reduce now problem (1) in the parallelepiped domain $\Omega = (0, L_x)\times(0, L_y)\times(0, L_z)$ of Figure 1, by assigning the homogeneous Robin data $\mu\nabla u\cdot\mathbf{n}+\chi u = 0$ on Γ_w. The problem data are again assumed constant. For this purpose, we generalize the procedure in the previous section to a 3D setting. In particular, to identify the educated modal basis associated with the selected boundary conditions, we solve the SLE problem (10) on the transverse fiber γ by taking advantage of the Cartesian structure of Ω. In this way problem (10) can be turned into a pair of one-dimensional SLE problems, whose solutions can be computed analytically. For complex geometries tensor product may be not an option. In this case, other solutions are demanded [14].

For simplicity, we set $\widetilde{\sigma} = 0$ in (8) since the reactive term just shifts the spectrum of the operator $\mathcal{L}_S$. Then, we factorize the eigenfunction in (10) as

$$\varphi_k(y, z) = \varphi_{y,p(k)}(y)\varphi_{z,q(k)}(z), \tag{26}$$

where $p(k)$ and $q(k)$ are indices related to the y- and to the z-coordinate, respectively used to identify the k-th 2D modal function φ_k. Factorization (26) leads to the one-dimensional eigenvalue problems

$$\begin{cases} -\mu\varphi''_{y,p(k)}(y) = \lambda_{y,p(k)}\varphi_{y,p(k)}(y) & \text{in } (0, L_y) \\ \mu\varphi'_{y,p(k)}(0) + \chi\varphi_{y,p(k)}(0) = 0 \\ \mu\varphi'_{y,p(k)}(L_y) + \chi\varphi_{y,p(k)}(L_y) = 0, \end{cases} \tag{27}$$

$$\begin{cases} -\mu\varphi''_{z,q(k)}(z) = \lambda_{z,q(k)}\varphi_{z,q(k)}(z) & \text{in } (0, L_z) \\ \mu\varphi'_{z,q(k)}(0) + \chi\varphi_{z,q(k)}(0) = 0 \\ \mu\varphi'_{z,q(k)}(L_z) + \chi\varphi_{z,q(k)}(L_z) = 0, \end{cases} \tag{28}$$

with $\lambda_{y,p(k)}$ and $\lambda_{z,q(k)}$ the eigenvalue associated with the eigenfunction $\varphi_{y,p(k)}$ and $\varphi_{z,q(k)}$, respectively. Thus, the eigenpair $(\varphi_k(y,z),\lambda_k)$ solution to the 2D problem (10) on the slice γ reads

$$(\varphi_k(y,z),\lambda_k) = (\varphi_{y,p(k)}(y)\varphi_{z,q(k)}(z), \lambda_{y,p(k)} + \lambda_{z,q(k)}). \tag{29}$$

Consistently with the analysis of the previous section, the eigenvalues λ_k have to be sorted into a non-decreasing sequence. We select indices $p(k)$ and $q(k)$ to identify the eigenvalue λ_k in (29) via the following algorithm hereafter denoted by ESA (Eigenvalue Sorting Algorithm).

Let m be given. Then, we perform the following steps.

i) For $k = 1$, we set $\lambda_1 = \lambda_{y,1} + \lambda_{z,1}$, i.e., $p(1) = 1$ and $q(1) = 1$ identify $k = 1$.
ii) While $k \leq m$, do
   - compute $\lambda_{y,p(k)+1} + \lambda_{z,q(k)}$ and $\lambda_{y,p(k)} + \lambda_{z,q(k)+1}$ and store these values in the list of the eigenvalues to examine;
   - compute the minimal element in the list of the eigenvalues to examine; this will be assigned to λ_{k+1}; correspondingly, we assign $p(k+1)$ and $q(k+1)$;
   - increment k.

A schematization of ESA is depicted in Figure 4. In particular, the diagram refers for simplicity to (27), for $L_y = \pi$ and $L_z = 3\pi/2$, completed with homogeneous Dirichlet boundary conditions, i.e., to a test case where the eigenvalues can be calculated exactly. The light-grey boxes refer to eigenvalues already examined, while the white boxes identify the eigenvalues that have to be still checked. In the boxes we report three numbers with the following notation $(\lambda_{y,p(k)}, \lambda_{z,q(k)})\boldsymbol{\lambda_k}$, while the numbers in brackets, outside the boxes, denote the index k.

When dealing with a 2D SLE problem, eigenvalues may have a multiplicity strictly greater than one. In the proposed algorithm, when this repetition occurs, either one of the repeated nodes or the other (see the dark-grey boxes in Figure 4) is removed from the list. For instance, in Figure 4, after the detection of the simple eigenvalue $\lambda_4 = 5$, we obtain the next candidate, i.e., the value 5.77, twice. Thus, one of the two occurrences is eliminated from the tree.

Remark 5 When fiber γ exhibits a dominant dimension, for instance, $L_y \gg L_z$, it is worth using a different number of modal basis functions along the direction y and z, respectively. In this case, the eigenvalues associated with z-direction are larger than the ones related to y-direction, as indicated by formula (12). Hence, since the truncation error scales with the inverse of the first truncated eigenvalue, less modal functions need to be employed along z-direction than y-direction. Thus, if the ratio L_z/L_y is significantly small, out of m modes we will select $m-1$ modes in the y-direction and a single mode along z, so that the tree of Figure 4 becomes extremely unbalanced, following only the y-side of the branch.

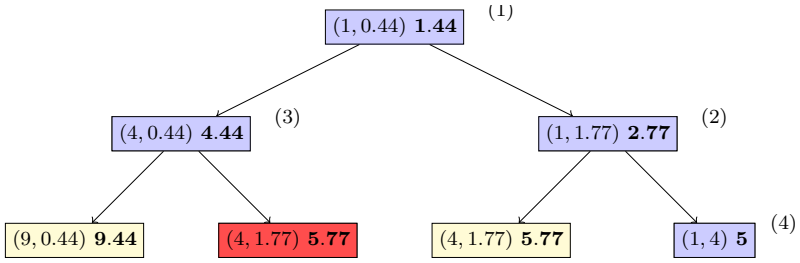

Fig. 4 Schematization of ESA to select the 2D eigenvalues λ_k in (29).

4.3 Error analysis

To analyze the error characterizing the e-HiMod reduction of problem (1), we first compute the error associated with the modal discretization (semi-discrete problem), and then we include the error due to the finite element approximation of the axial dynamics.

As for the semi-discretization error, we have the following result.

Theorem 3 *Let $u \in H^2(\Omega)$ be the weak solution to the full problem (1), with $\Omega \subset \mathbb{R}^d$, and let $P_m u$ denote the orthogonal projection of u onto the HiMod space V_m in (3), being $\{\varphi_k\}_{k=1}^m$ an educated modal basis. Then, there exists a constant $\widetilde{C}_{1,s}$, independent of m, such that, for $s = 0, 1$,*

$$||u - P_m u||_{H^s(\Omega)} \leq \widetilde{C}_{1,s} \left(\frac{1}{m+1}\right)^{\frac{2-s}{d-1}} \|u\|_{H^2(\Omega)}. \tag{30}$$

Moreover, if $u \in H^{2p}(\Omega)$, with $p \geq 2$, and $\mathcal{L}_S^r u$ satisfies compatible boundary conditions up to order $p-1$, then there exists a constant $\widetilde{C}_{2,s}$, independent of m, such that, for $s = 0, 1$,

$$||u - P_m u||_{H^s(\Omega)} \leq \widetilde{C}_{2,s} \left(\frac{1}{m+1}\right)^{\frac{2p-s}{d-1}} ||u||_{H^{2p}(\Omega)}. \tag{31}$$

Proof By exploiting the density of the space V_∞ in V for the modal representation of u, we have

$$\begin{aligned} ||u - P_m u||^2_{L^2(\Omega)} &= \int_{\Omega_{1D}} \int_\gamma \left[\sum_{k=m+1}^{+\infty} u_k(x)\varphi_k(\mathbf{y}) \right]^2 d\mathbf{y}dx \\ &= \int_{\Omega_{1D}} ||\big(u - P_m u\big)(x)||^2_{L^2(\gamma)}\, dx. \end{aligned}$$

Estimates (30) and (31) for $s = 0$ now follow from Theorem 1, after identifying $\mathcal{R}_m f$ with $\big(u - P_m u\big)(x)$. Similar arguments can be used for the error estimates with respect to the $H^1(\Omega)$-norm.

□

Now, we consider the fully discretized solution u_m^h, obtained by completing the modal expansion with an approximation of the axial dynamics via finite elements. So far we have assumed to employ a piecewise linear discretization along Ω_{1D}. The next results are more general and refer to finite elements of generic order r.

Theorem 4 *Let $u \in H^s(\Omega)$, with $s \geq 2$, be the weak solution to the full problem* (1)*, with $\Omega \subset \mathbb{R}^d$. Then, the error associated with the e-HiMod reduction satisfies the* a priori *estimate*

$$\|u - u_m^h\|_{H^1(\Omega)} \leq C(h^q + m^{-l})\|u\|_{H^s(\Omega)}, \tag{32}$$

with $q = \min(s-1, r)$ and $l = 1/(d-1)$. In particular, if $u \in H^{2p}(\Omega)$, with $p \geq 2$, and $\mathcal{L}_S^r u$ satisfies compatible boundary conditions up to order $p-1$, then $l = (2p-1)/(d-1)$.

Proof Via Céa's Lemma and the triangle inequality, it follows

$$\begin{aligned}\|u - u_m^h\|_{H^1(\Omega)} &\leq C \inf_{v_m^h \in V_m^h} \|u - v_m^h\|_{H^1(\Omega)} \\ &\leq C\left(\|u - v_m\|_{H^1(\Omega)} + \|v_m - v_m^h\|_{H^1(\Omega)}\right),\end{aligned}$$

where $v_m \in V_m$ is the semi-discrete counterpart of the generic e-HiMod function v_m^h. Now, we identify v_m with $P_m u$. As a consequence, the thesis promptly follows from classical piecewise polynomial approximation results [10] and from Theorem 3.

□

With similar arguments from Theorem 2 for the specific case of Neumann data, we have the following result (we do not report the proof for brevity):

Theorem 5 *Let $u \in H^4(\Omega)$ be the weak solution to the full problem* (1) *completed with homogeneous Neumann conditions on Γ_w and homogeneous Dirichlet data on $\Gamma_1 \cup \Gamma_2$, with $\Omega \subset \mathbb{R}^d$. Let $P_m u$ be defined as in Theorem 3. Then, there exists a constant $\widetilde{C}_{3,s}$ independent of m, such that, for $s = 0, 1$,*

$$||u - P_m u||_{H^s(\Omega)} \leq \widetilde{C}_{3,s}\left(\frac{1}{m+1}\right)^{\frac{3-s}{d-1}} \|u\|_{H^4(\Omega)}.$$

In addition, if the modal functions $\{\varphi_k\}_k$ are uniformly bounded with respect to k, then there exists a constant $\widetilde{C}_{4,s}$, independent of m, such that

$$||u - P_m u||_{H^s(\Omega)} \leq \widetilde{C}_{4,s}\left(\frac{1}{m+1}\right)^{\frac{4-s}{d-1}} \|u\|_{H^4(\Omega)}.$$

Thus, if $u \in H^s(\Omega)$, with $s \geq 2$, the error associated with the e-HiMod reduction procedure satisfies the a *priori estimate*

$$\|u - u_m^h\|_{H^1(\Omega)} \leq C(h^q + m^{-l})\|u\|_{H^s(\Omega)}, \tag{33}$$

with $q = \min(s-1, r)$ and $l = (3-s)/(d-1)$ (or $l = (4-s)/(d-1)$ for uniformly bounded modal basis functions).

Remark 6 Under suitable assumptions on the boundary $\partial\Omega$ of Ω and on the boundary data, estimates (32) and (33) can be generalized to control the $L^2(\Omega)$-norm of the global error $u - u_m^h$, with the expected orders $q+1$ and $l+1$.

Remark 7 When numerically computing the educated modal basis, errors may induce a loose of orthogonality. This reflects into an additional error component. In practice, the numerical modal approximation $\tilde{u}_m$ of u_m may not coincide with the orthogonal projection $P_m u$. In fact, the coefficients of the expansion of $\tilde{u}_m$ on the selected basis are affected by an error due to the terms (φ_i, φ_j) for $i \neq j$. In this case, denoting by ε the orthogonality error ($\varepsilon \leq \max_{ij} |(\varphi_i, \varphi_j)|$), we argue that the error $u - u_m^h$ features an additional component proportional to $\varepsilon\lambda_1^{-1}$. In our numerical results the impact of this error never prevented the convergence of the scheme, as we verified that ε is significantly smaller than the discretization error.

5 Numerical assessment of the e-HiMod procedure

We consider both 2D and 3D test cases. The two-dimensional e-HiMod code is developed in `Matlab`, while the 3D tests are implemented in `LifeV` [17]. Numerical results are validated against analytical solutions when available, and finite element approximations on fine enough meshes otherwise.

5.1 Verification

We start by qualitatively investigating the consistency of the e-HiMod procedure with a reference finite element solution computed on a fine mesh in absence of an analytical solution. In particular, we focus on a 2D setting and we consider different choices for the boundary data.
Let us consider the problem

$$\begin{cases} -\Delta u + \boldsymbol{\beta} \cdot \nabla u = f & \text{in } \Omega = (0,6) \times (0,1) \\ u = g_D & \text{on } \Gamma_{in} \\ \nabla u \cdot \mathbf{n} + \chi u = g_R & \text{on } \Gamma_{out} \\ \rho_1 \nabla u \cdot \mathbf{n} + \rho_2 u = 0 & \text{on } \Gamma_{up} \cup \Gamma_{down}, \end{cases} \tag{34}$$

where $\boldsymbol{\beta} = (20, 0)^T$ represents a horizontal wind, $\Gamma_{in} = \{0\} \times [0,1]$, $\Gamma_{out} = \{6\} \times [0,1]$, g_D and g_R are given functions, χ is a constant, and the forcing term f models two elliptical sources localized in the left-portion of the domain, being $f(x,y) = \chi_{E_1 \cup E_2}(x,y)$, with $E_1 = \{(x,y) \in \Omega : (x-1.5)^2 + 0.4(y-0.25)^2 \leq 0.01\}$ and $E_2 = \{(x,y) \in \Omega : (x-1.5)^2 + 0.4(y-0.75)^2 \leq 0.01\}$ (see Figure 5). Condition on $\Gamma_w = \Gamma_{up} \cup \Gamma_{down}$ prescribes Robin, Dirichlet or Neumann data according to the parameters ρ_1, ρ_2, which can take different values on different portions of the lateral boundary, being $\Gamma_{up} = [0,6] \times \{1\}$ and $\Gamma_{down} = [0,6] \times \{0\}$.

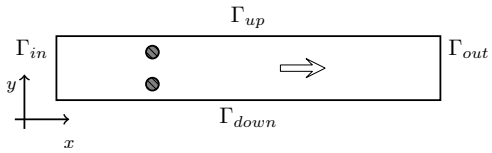

Fig. 5 Schematization of the 2D test case setting for the e-HiMod verification.

We test two combinations of boundary conditions on Γ_{up} and Γ_{down}, i.e., Dirichlet/Robin and Robin/Robin data, respectively. At the intersection of the different portions of the boundary, data are prescribed to be compatible. As reference solution, we take the continuous piecewise linear approximation computed on a structured uniform grid with mesh sizes $h_x = h_y = 0.0025$. Concerning the e-HiMod approximation, we adopt linear finite elements to discretize Ω_{1D}, being $\mathcal{T}_h$ a uniform partition of step $h = 0.01$, while varying the number of educated modes along γ.

Dirichlet/Robin data - We assign the Robin condition $\nabla u \cdot \mathbf{n} = -3(u - 0.06)$ on Γ_{down}, and the Dirichlet data $u = 0.05$ on Γ_{up}. In Figure 6, top we show the contour plot of the reference finite element approximation. The Robin data on Γ_{down} warps downward the horizontal dynamics induced by the wind, so the effect of the two forcing terms on the solution is different and clearly detectable.

We compute the e-HiMod approximation by gradually increasing the modal index m. We adopt the notation e-Himod(m) to denote the hierarchically reduced solution associated with m educated modal functions. Figure 6 shows the contour plot of the e-HiMod(m) approximation, for $m = 2, 4, 8$. As expected, the quality of the reduced solution improves when m increases. For $m = 8$, the solution fully overlaps to the reference one.

Robin/Robin data - We now assign non-homogeneous Robin conditions on both Γ_{up} and Γ_{down}, namely we impose $\nabla u \cdot \mathbf{n} = -3(u - 0.06)$ on Γ_{up} and $\nabla u \cdot \mathbf{n} = -3(u - 0.05)$ on Γ_{down}, respectively.

In Figure 7 we compare the e-HiMod(m) approximation corresponding to $m = 2, 4, 8$ (second-fourth row) with the reference solution (first row). Due to the nontrivial trend of the solution, in this case $m = 4$ still provides an inaccurate solution, while the inclusion of four more modes provides an accurate solution, as shown in the last row of the figure.

Space-dependent coefficients - In Figure 8 we finally demonstrate the consistency of the e-HiMod procedure when dealing with non-constant coefficients. In this case, we add the reactive term σu in (34), where the coefficient σ coincides with the characteristic function associated with two circular subsets of the domain. The same Robin data is assigned on Γ_{up} and Γ_{down}, while the source term f is set equal to zero. Also in this case, the convergence of the e-HiMod solution to the reference one is evident when m increases.

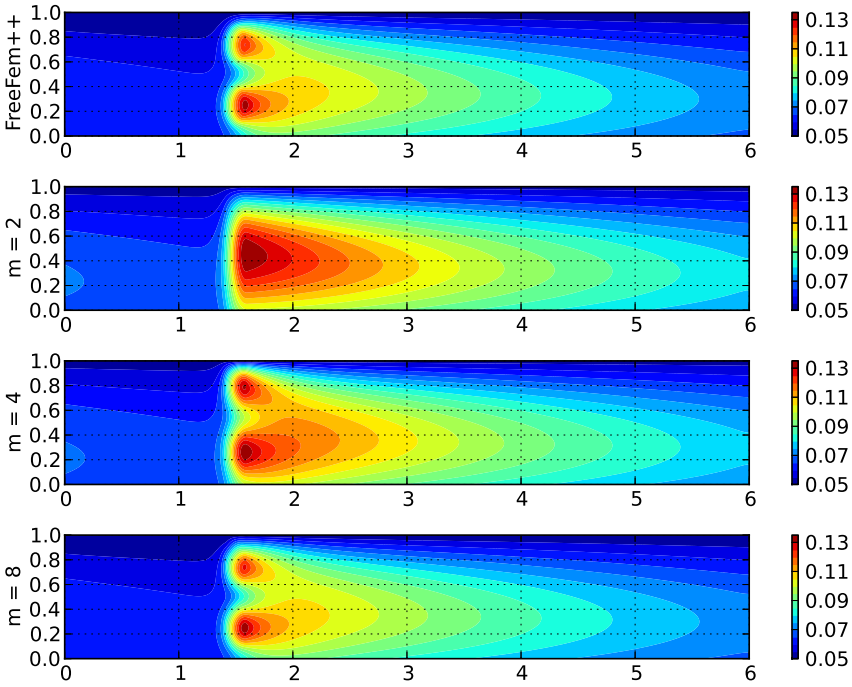

Fig. 6 Dirichlet/Robin data: reference finite element solution (top); e-HiMod(m) reduced solution for $m = 2$, 4, 8 (second-fourth row).

5.2 Effectiveness

We quantify the effectiveness of the e-HiMod reduction procedure with respect to a standard 2D finite element approximation in terms of number of degrees of freedom (dof). We consider problem (34) by assigning the non-homogeneous Robin conditions $\nabla u \cdot \mathbf{n} = -3(u - 0.06)$ on Γ_{up} and $\nabla u \cdot \mathbf{n} = -3(u - 0.05)$ on Γ_{down}, respectively while selecting $f = 10\chi_{F_1 \cup F_2}(x, y)$, with $F_1 = \{(x, y) \in \Omega : (x - 3)^2 + 0.4(y - 0.25)^2 \leq 0.01\}$ and $F_2 = \{(x, y) \in \Omega : (x - 1.5)^2 + 0.4(y - 0.75)^2 \leq 0.01\}$. Notice that the two sources are not aligned with any of the Cartesian axes.

When the leading dynamics is aligned with the supporting fiber Ω_{1D}, the e-HiMod approach effectively reduces the number of dof, without giving up accuracy. To show this, we compute: a high-resolution linear finite element approximation based on a uniform structured mesh of sizes $h_x = 0.01$, $h_y = 0.01$ (Figure 9, first row); a low-resolution linear finite element approximation obtained by increasing h_y to 0.2 (Figure 9, second row); the e-HiMod(m) approximation associated with $m = 1$ (Figure 9, fourth row) and $m = 5$ (Figure 9, fifth row), with $\mathcal{T}_h$ a uniform partition of Ω_{1D} of step size $h = 0.01$ in both the cases. Consequently, the number of dof of the four approximations is 60000

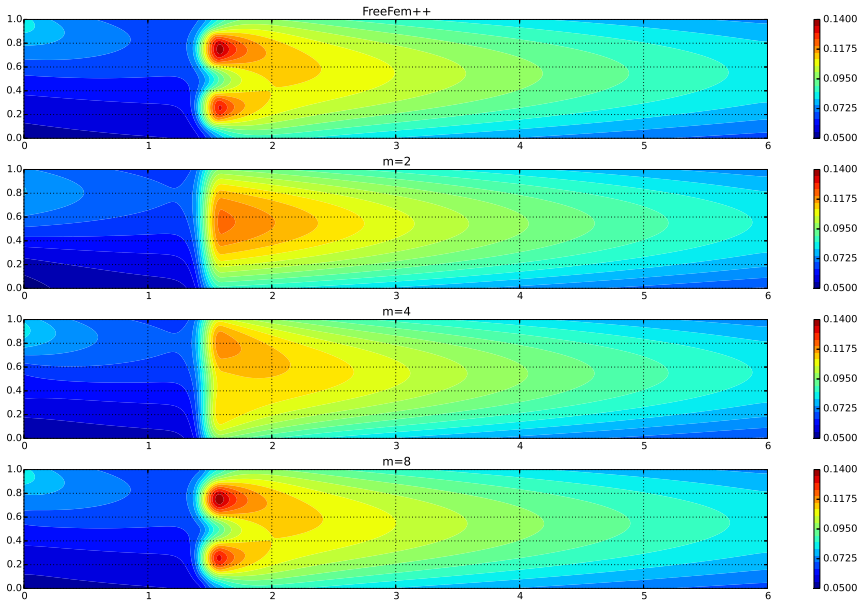

Fig. 7 Robin/Robin data: reference finite element solution (top); e-HiMod(m) reduced solution for $m = 2$, 4, 8 (second-fourth row).

(high-resolution reference solution), 3000 (low-resolution reference solution), 600 (e-HiMod(1)) and 3000 (e-HiMod(5)), respectively.
The e-HiMod(5) approximation perfectly matches the high-resolution reference approximation, albeit obtained by solving a linear system whose dimension is 20 times smaller compared with the finite element one. Conversely, the low-resolution finite element approximation demands exactly the same number of dof as the e-HiMod(5) solution but with an evident lower accuracy.
Finally, as expected, the e-HiMod(1) model is too coarse due to the limited transverse information carried by a single mode. Nevertheless, we point out how the e-HiMod(1) solution is more informative than the transverse-averaged finite element solution in Figure 9, third row, obtained by averaging the 2D ADR problem along the transverse direction. In particular, we compute the averaged solution by preserving the partition along Ω_{1D} of size $h = 0.01$, still resulting in 600 dof. This confirms the results in [2], where the HiMod approach is compared with the Geometrical Multiscale Approach [30], coupling dimensionally heterogeneous problems to cover large portions of a pipe network. The e-HiMod approach provides surrogate approximations (like purely

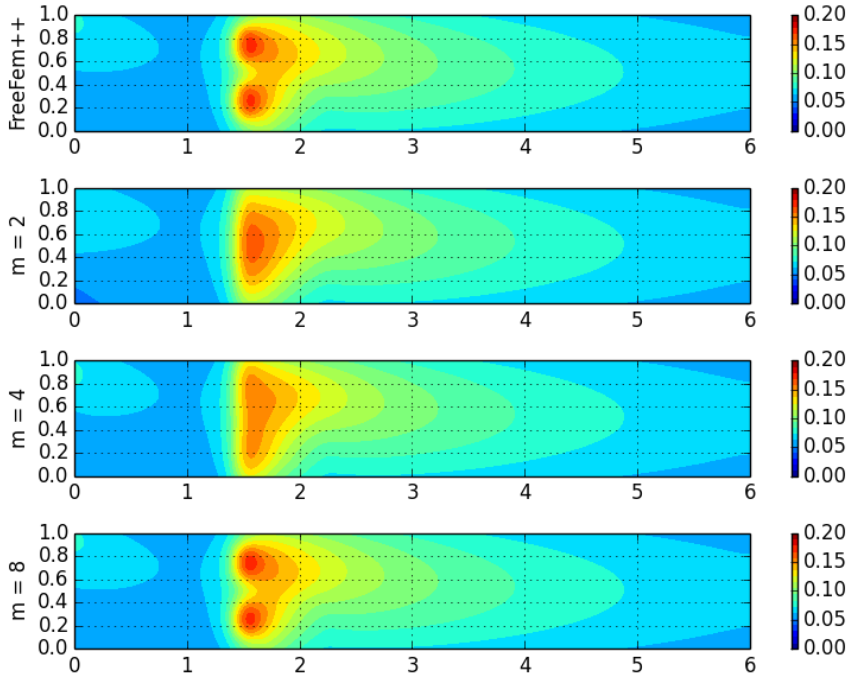

Fig. 8 Space-dependent coefficients: reference finite element solution (top); e-HiMod(m) reduced solution for $m = 2, 4, 8$ (second-fourth row).

one-dimensional models) yet amenable to be locally (and promptly) refined, with computational costs that outperform traditional approaches.

5.3 Educated vs non-educated modal bases

This section highlights the added value provided by an educated modal basis with respect to a standard Fourier basis. For the sake of simplicity, this check is performed in a 2D framework. To this aim, we consider the ADR problem

$$\begin{cases} -\Delta u + \boldsymbol{\beta} \cdot \nabla u + \sigma u = f & \text{in } \Omega = (0,1)^2 \\ u = u_{ex} & \text{on } \Gamma_{in} \\ \nabla u \cdot \mathbf{n} = \nabla u_{ex} \cdot \mathbf{n} & \text{on } \Gamma_{out} \\ \nabla u \cdot \mathbf{n} + 3u = 0 & \text{on } \Gamma_{up} \cup \Gamma_{down}, \end{cases} \tag{35}$$

with $\boldsymbol{\beta} = (20, 0)^T$, $\sigma = 2$, $\Gamma_{in} = \{0\} \times [0,1]$, $\Gamma_{out} = \{1\} \times [0,1]$, $\Gamma_{down} = [0,1] \times \{0\}$, $\Gamma_{up} = [0,1] \times \{1\}$. The source term is selected so that the analytical

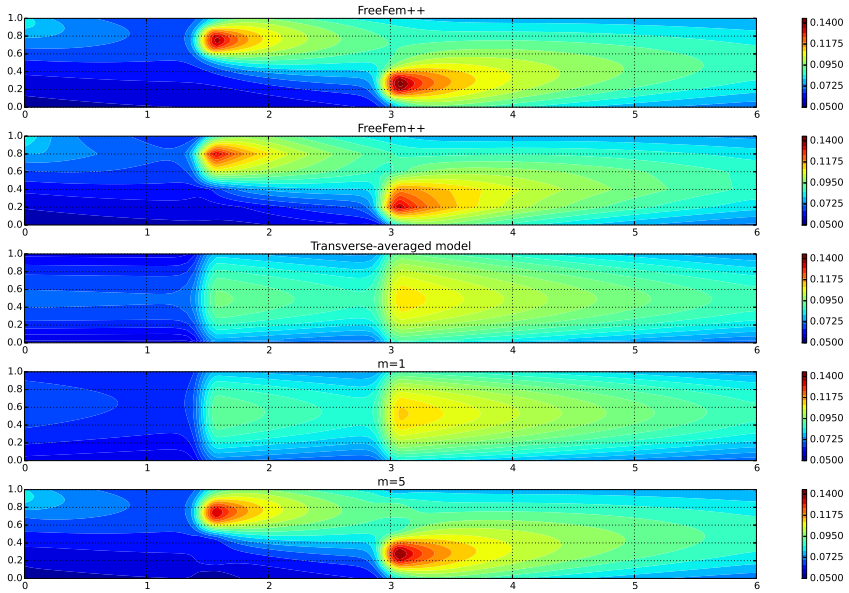

Fig. 9 Robin/Robin data: comparison among 2D linear finite element discretizations (first and second row), the transverse-averaged ADR model (third row), and the e-HiMod(1) and e-HiMod(5) approximations (fourth and fifth row).

solution is

$$u_{ex} = xy + x + y + \exp(2xy - y) - 1 \\ - y^2\big[2x + \exp(2x-1) + 0.1((4x-6)\exp(2x-1) - 6x + 2)\big].$$

In Figure 10, left we provide the contour plot of u_{ex}. One possibility is to resort to the Fourier basis $\mathcal{F}_m = \{1, \cos(j\pi y), \sin(j\pi y)\}_{j=1}^m$ and to a natural treatment of the boundary conditions. This is expected to introduce some error as opposed to the essential treatment of the same conditions with an educated basis. This is confirmed by the contour plots in Figure 10, center and right associated with the basis $\mathcal{F}_4$ and with the e-HiMod(4) solution, respectively. While this last approximation matches the exact solution, the standard HiMod solution based on $\mathcal{F}_4$ exhibits a significant discrepancy to u_{ex}.

We compare also the convergence of the two HiMod approximations. In Figure 11 we show the convergence rate of the global error with respect to the $L^2(\Omega)$- (left) and the $H^1(\Omega)$-norm (right), for both the educated and the non-educated modal bases. Convergence is attained by both the approaches, even though the HiMod reduction based on $\mathcal{F}_m$ is definitely slower compared with the e-HiMod approach. In particular, the Fourier basis leads to a linear

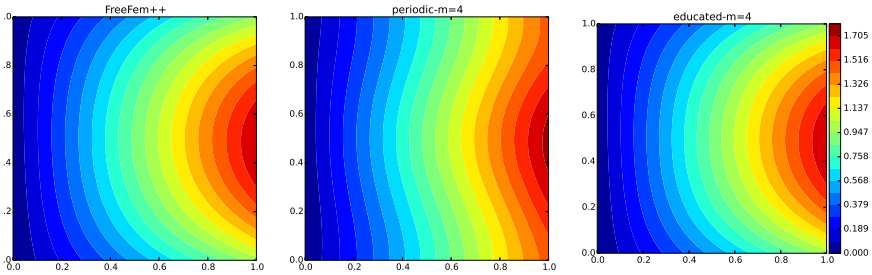

Fig. 10 Educated vs non-educated modal bases: exact solution to problem (35) (left); HiMod approximation based on $\mathcal{F}_4$ (center); e-Himod(4) approximation (right).

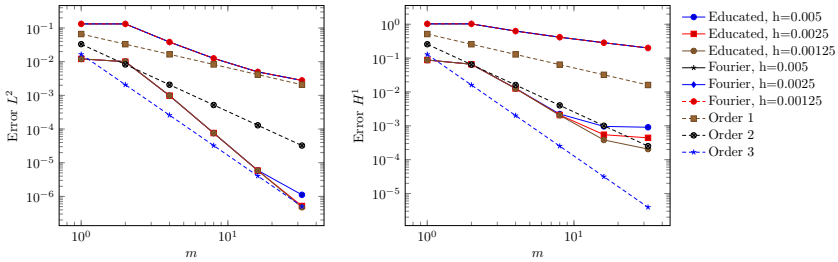

Fig. 11 Educated vs non-educated modal bases: convergence rate of the global error with respect to the $L^2(\Omega)$-norm (left) and $H^1(\Omega)$-norm (right), for different discretization steps.

convergence for the $L^2(\Omega)$-norm, and to a sub-linear rate with respect to the $H^1(\Omega)$-norm. Moreover, no sensitivity with respect to h can be appreciated, suggesting that the modal error dominates the one due to the finite element discretization.
Theorem 4 predict a quadratic and a linear convergence rate for the global error of the e-HiMod approximation with respect to the $L^2(\Omega)$- and the $H^1(\Omega)$-norm, respectively. Actually, results in Figure 11 slightly outperform the expected convergence rate in the range of the selected modes.

5.4 Convergence analysis

We complete the qualitative analysis in the previous sections with a more quantitative investigation, by assessing the convergence rate of the e-HiMod approximation. To this aim, we select a step h small enough to emphasize the modal error, or, alternatively, a large number m of modes to highlight the finite element approximation error. We consider both 2D and 3D cases. All the convergence graphs provided hereafter are log-log plots.

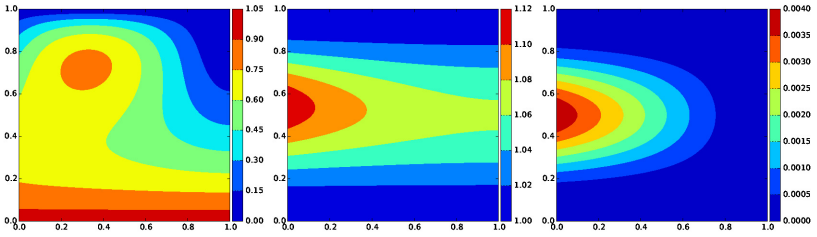

Fig. 12 2D convergence analysis: exact solution to problem (36) completed with Dirichlet/Robin (left), Neumann/Neumann (center), and compatible (right) boundary data.

5.4.1 2D analysis

We consider different choices for the boundary data to be assigned on Γ_w.

Dirichlet/Robin data - The first case test solves the ADR problem

$$\begin{cases} -\Delta u + \boldsymbol{\beta} \cdot \nabla u + \sigma u = f & \text{in } \Omega = (0,1)^2 \\ u = u_{ex} & \text{on } \Gamma_{in} \\ u = 0 & \text{on } \Gamma_{up} \\ \nabla u \cdot \mathbf{n} + u = 3 & \text{on } \Gamma_{down} \\ \nabla u \cdot \mathbf{n} = 0 & \text{on } \Gamma_{out}, \end{cases} \tag{36}$$

with $\boldsymbol{\beta} = (20, 0)^T$, $\sigma = 2$, $\Gamma_{in} = \{0\} \times [0,1]$, $\Gamma_{out} = \{1\} \times [0,1]$, $\Gamma_{down} = [0,1] \times \{0\}$, $\Gamma_{up} = [0,1] \times \{1\}$, and f such that the analytical solution is $u_{ex} = 4y^2(1-y)(0.75 + 8x^2y + 8xy^2)(x-1)^2 + (1-y)^2$ (see Figure 12, left).

The results of the convergence analysis are summarized in Figure 13 and quantified in Table 1 and 2, where we evaluate the global error with respect to the $L^2(\Omega)$- and the $H^1(\Omega)$-norm, respectively. The step size h characterizing $\mathcal{T}_h$ is gradually halved, starting from the value 0.1; conversely, the modal index m is doubled, starting from a single mode. For h small enough, modal approximation slightly outperforms the expected convergence rates (error reduction factors are about 5 and 2.5 versus the expected 4 and 2, respectively). This is most likely related to the regularity of the solution. For the largest values of h, we have a slight stagnation of the error, in particular with respect to the $H^1(\Omega)$-norm. The error dependence on h is evident only for high values of m, as the modal error dominates.

Neumann/Neumann data - We check the results of Theorem 5. For this purpose, we replace in (36) the conditions on Γ_{up} and Γ_{down} with a homogeneous Neumann data, while preserving the condition on Γ_{in} and the free-flux condition on Γ_{out}. Thus, the exact solution is $u_{ex} = y^2(1-y)^2 \exp\big(\sin(20y^3(1-y)^2(x-1)^2)\big)$ (see Figure 12, center). Theorem 5 predicts order 4 and 3 with

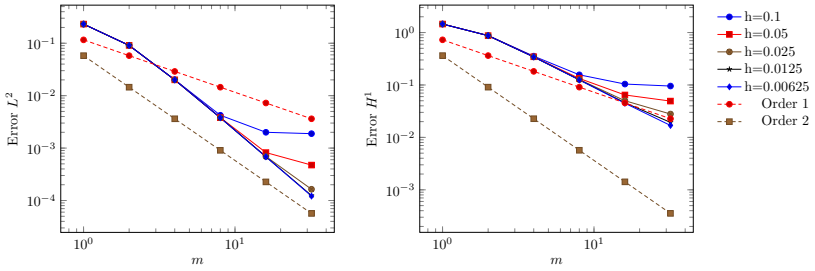

Fig. 13 2D convergence analysis, Dirichlet/Robin data: global error with respect to the $L^2(\Omega)$-norm (left) and $H^1(\Omega)$-norm (right), for different discretization steps.

m	h=0.1	h=0.05	h=0.025	h=0.0125	h=0.00625
1	2.32e-01	2.32e-01	2.32e-01	2.32e-01	2.32e-01
2	9.09e-02	9.08e-02	9.08e-02	9.08e-02	9.08e-02
4	2.01e-02	2.00e-02	2.00e-02	2.00e-02	2.00e-02
8	4.23e-03	3.82e-03	3.79e-03	3.79e-03	3.79e-03
16	2.00e-03	8.22e-04	6.91e-04	6.83e-04	6.82e-04
32	1.88e-03	4.74e-04	1.64e-04	1.24e-04	1.21e-04

Table 1 2D convergence analysis, Dirichlet/Robin data: global error with respect to the $L^2(\Omega)$-norm.

m	h=0.1	h=0.05	h=0.025	h=0.0125	h=0.00625
1	1.45e+00	1.45e+00	1.45e+00	1.45e+00	1.45e+00
2	8.77e-01	8.74e-01	8.73e-01	8.73e-01	8.73e-01
4	3.55e-01	3.45e-01	3.43e-01	3.42e-01	3.42e-01
8	1.56e-01	1.33e-01	1.27e-01	1.25e-01	1.25e-01
16	1.04e-01	6.45e-02	5.01e-02	4.58e-02	4.49e-02
32	9.54e-02	4.93e-02	2.79e-02	1.93e-02	1.69e-02

Table 2 2D convergence analysis, Dirichlet/Robin data: global error with respect to the $H^1(\Omega)$-norm.

respect to the $L^2(\Omega)$- and the $H^1(\Omega)$-norm, respectively. In Figure 14 we provide the plot of the global error as a function of m and for decreasing values of h. The plots associated with different mesh sizes are perfectly overlapped until 16 educated modes are used. The error stagnates except for the smallest values of h, showing a dominance of the finite element discretization error. For $h = 0.0125, 0.00625, 0.003125$, the $L^2(\Omega)$-norm of the error shows the expected order of convergence, while the choices $h = 0.00625$, $h = 0.003125$ show the rate predicted by Theorem 5 for the $H^1(\Omega)$-norm. Finally, as for the Dirichlet/Robin data, the $H^1(\Omega)$-norm exhibits a minor sensitivity to the step size h.

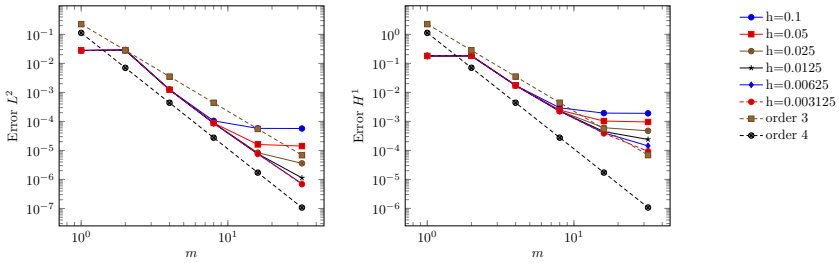

Fig. 14 2D convergence analysis, Neumann/Neumann data: global error with respect to the $L^2(\Omega)$-norm (left) and $H^1(\Omega)$-norm (right), for different discretization steps.

Compatible data - We solve problem (36) by assigning homogeneous Dirichlet boundary conditions on $\Gamma_{up} \cup \Gamma_{down}$. Thus, the exact solution coincides with $u_{ex} = y^4(1-y)^4 e^x (x-1)^2$ (see Figure 12, right). This function satisfies compatible boundary conditions. In particular, the Laplacian of u is identically equal to zero on Γ_{up} and Γ_{down}, so that we expect a superconvergent trend when evaluating the global error with respect to the $L^2(\Omega)$- and the $H^1(\Omega)$-norm, consistently with the results in Theorem 4. This behavior is confirmed by Figure 15. The convergence rate for the $L^2(\Omega)$-norm is about 4 for h sufficiently small, as stated in (32). Concerning the $H^1(\Omega)$-norm, the finite element error induces a stagnation, preventing to neatly appreciate the expected modal error convergence rate.

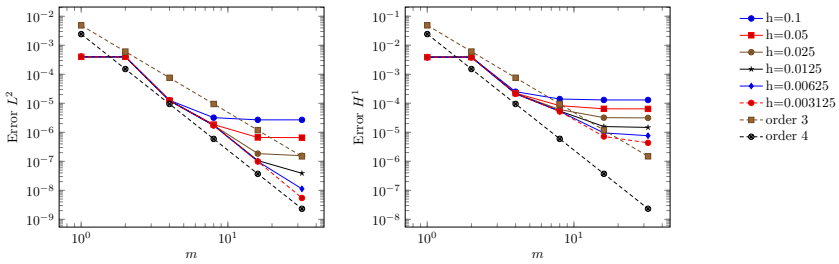

Fig. 15 2D convergence analysis, compatible data: global error with respect to the $L^2(\Omega)$-norm (left) and $H^1(\Omega)$-norm (right), for different discretization steps.

5.4.2 3D analysis

We extend the investigation of the previous section to a 3D setting, in particular by focusing on the $L^2(\Omega)$-norm. As for the 2D case, we consider different choices for the boundary conditions to be assigned on Γ_w.

Dirichlet data - We solve problem (1) on $\Omega = (0, 0.2) \times (0, 0.1)^2$, with $\mu = 1$, $\boldsymbol{\beta} = (5, 1, 1)^T$ and $\sigma = 3$. We impose homogeneous Dirichlet data on the whole

Γ_w, while we assign a Dirichlet data on Γ_1 and a homogeneous Neumann boundary condition on Γ_2. In particular, we select the source term and the Dirichlet condition on Γ_1 so that the exact solution is $u_{ex}(x,y,z) = 10^7 y(0.1-y)z(0.1-z)(x-0.2)^2\exp(2yz(0.2-x)^2)$. As for the 2D analysis, we make different choices for the (uniform) spacing step along the supporting fiber Ω_{1D}, and then, for each selected h, we gradually increase the number of modal functions.
Figure 16, left shows the trend of the global error for five choices of h. The modal order of convergence predicted for the $L^2(\Omega)$-norm by the theory in Section 4 is 1. This is approximatively what we infer from the results in the figure, when the finite element error does not dominate.

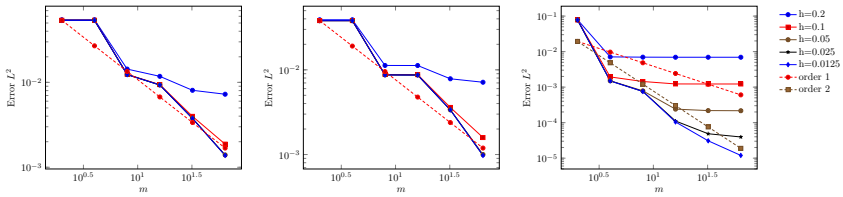

Fig. 16 3D convergence analysis: global error with respect to the $L^2(\Omega)$- and $H^1(\Omega)$-norm for different discretization steps, in the presence of Dirichlet (left), Dirichlet/Robin (center) and Robin (right) data.

Dirichlet/Robin data - We solve the standard Poisson problem on the cube $\Omega = (0, 0.1)^3$, by assigning a homogeneous Dirichlet data on the upper and on the lower faces, Γ_{up} and Γ_{down}, and the homogeneous Robin condition $\nabla u \cdot \mathbf{n} + 3.345u = 0$ on Γ_w. The source term is selected such that the exact solution is $u_{ex}(x,y,z) = 10^5(0.1-x)^2 z(0.1-z)\exp\left(70y^2/(xz+1) - 140y^3/(0.3(xz+1)) - 3.345(0.1-2y)^2/(0.4\mu)\right)$. As shown in Figure 16, center the $L^2(\Omega)$-norm of the global error exhibits a rate very similar to the one characterizing the fully Dirichlet case, showing how the e-HiMod approach does successfully extend the results derived for the Dirichlet case. In particular, for m sufficiently large and for h small enough, we obtain the expected rate of convergence, with a slight superconvergence for $h = 0.025$ and $h = 0.0125$.

Robin data - We modify the previous test case by assigning now a full Robin boundary condition $\nabla u \cdot \mathbf{n} + 4.456u = 0$ on the entire surface $\partial\Omega$. We observe more sensitivity to the selected step size h with respect to the previous choices of boundary conditions (compare the panel in Figure 16, right with the two others). To check the modal convergence, we analyze the plot associated with $h = 0.0125$ which essentially exhibit the expected linear rate, with a slight superconvergent trend. This can be likely justified by the fact that Robin conditions here quantitatively approaches Neumann conditions, which yield superconvergence, as for Theorem 5.

5.5 The backward facing step test case

We conclude the numerical assessment of this section by analyzing the robustness of the e-HiMod approach on a more complex configuration. In particular, we focus on a backward-facing step geometry, both in 2D and in 3D.

5.5.1 The 2D case

We identify the computational domain Ω in (1) with the L-shaped portion $\Omega_q \setminus \Omega_l$ of the Cartesian plane, being $\Omega_q = (0,2) \times (-1,1)$ and $\Omega_l = (0,1) \times (-1,0)$. Moreover, we distinguish the following portions of the boundary $\partial\Omega$: $\Gamma_{in} = \{0\} \times [0,1]$ and $\Gamma_{out} = \{2\} \times [-1,1]$ coinciding with the inlet and the outlet, respectively; $\Gamma_{up} = [0,2] \times \{1\}$ and $\Gamma_{down} = [1,2] \times \{-1\} \cup \{1\} \times [-1,0]$ to denote the upper and lower portion of the boundary, respectively. On this domain we solve the advection-diffusion problem

$$\begin{cases} -\Delta u + \boldsymbol{\beta} \cdot \nabla u = f & \text{in } \Omega \\ u = y(1-y) & \text{on } \Gamma_{in} \\ \nabla u \cdot \mathbf{n} = 0 & \text{on } \Gamma_{out} \\ \nabla u \cdot \mathbf{n} + u = 0 & \text{on } \Gamma_{up} \\ u = 0 & \text{on } \Gamma_{down}, \end{cases} \tag{37}$$

where the source term is $f(x,y) = 10\chi_{G_1 \cup G_2}(x,y)$, with $G_1 = \{(x,y) \in \Omega : (x-1.5)^2 + 0.4(y-0.25)^2 \leq 0.01\}$ and $G_2 = \{(x,y) \in \Omega : (x-1.5)^2 + 0.4(y-0.75)^2 \leq 0.01\}$, while the advective field $\boldsymbol{\beta}$ is the solution to the Stokes problem

$$\begin{cases} -\nabla \cdot \mathbf{T}(\boldsymbol{\beta}, p) = 0 & \text{in } \Omega \\ \nabla \cdot \boldsymbol{\beta} = 0 & \text{in } \Omega \\ \mathbf{T}(\boldsymbol{\beta}, p)\mathbf{n} = 5\mathbf{n} & \text{on } \Gamma_{in} \\ \mathbf{T}(\boldsymbol{\beta}, p)\mathbf{n} = \mathbf{0} & \text{on } \Gamma_{out} \\ \boldsymbol{\beta} = \mathbf{0} & \text{on } \Gamma_w = \Gamma_{up} \cup \Gamma_{down}, \end{cases} \tag{38}$$

with $\mathbf{T} = \nu(\nabla\boldsymbol{\beta} + \nabla\boldsymbol{\beta}^T) - pI$ the stress rate tensor depending on the velocity $\boldsymbol{\beta}$ and on the pressure p, being $\nu > 0$ the kinematic viscosity and I the identity matrix. Figure 17, bottom-left shows the contour plot of a reference solution to problem (37) computed via linear finite elements on a structured uniform mesh of sizes $h_x = h_y = 0.01$. The same mesh has been employed to compute $\boldsymbol{\beta}$ via a P2-P1 finite element scheme. Figure 17, top shows the x- and y-component of such a field.

To approximate problem (37) via an e-HiMod procedure, we resort to the piecewise HiMod formulation [24]. Following this approach, we split Ω into the two subdomains $\Omega_1 = (0,1)^2$ and $\Omega_2 = (1,2) \times (-1,1)$, and we apply, on each of them, the standard e-HiMod reduction. Then, the two reduced models are merged via a domain decomposition iterative scheme. In particular, we adopt a relaxed Dirichlet/Neumann scheme in correspondence with the

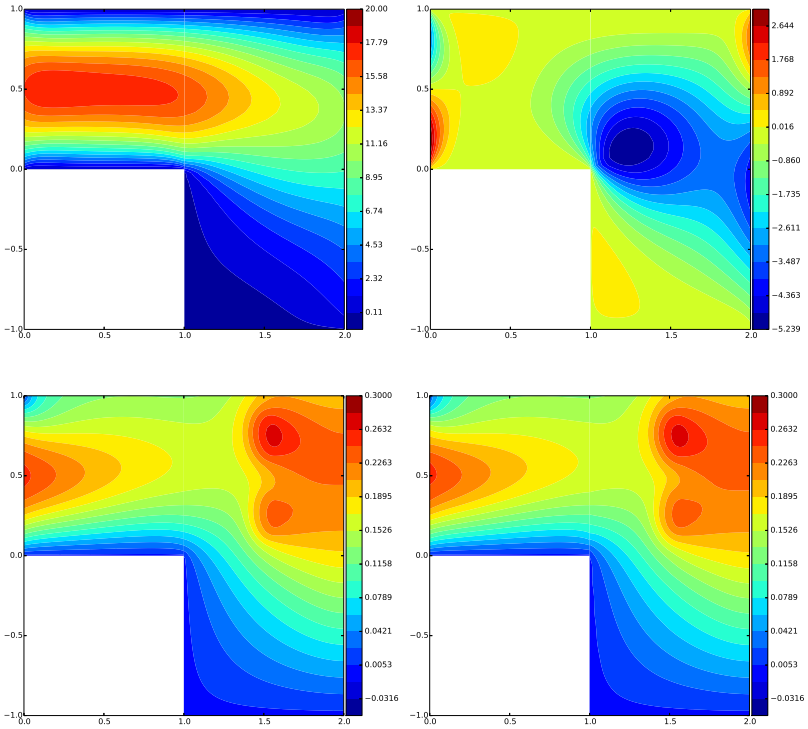

Fig. 17 2D backward facing step: x-component (top-left) and y-component (top-right) of the advective field $\boldsymbol{\beta}$; reference finite element approximation (bottom-left); piecewise e-HiMod$(8, 20)$ reduced solution (bottom-right).

interface $\Gamma = \{1\} \times (0, 1)$ between Ω_1 and Ω_2. We use 8 and 20 educated modal functions on Ω_1 and Ω_2, respectively while introducing a uniform subdivision along the supporting fiber Ω_{1D} of step-length $h_x = 0.01$.

The corresponding reduced solution, denoted by e-HiMod$(8, 20)$, is shown in Figure 17, bottom-right. It compares very well with the reference finite element approximation, yet with a significant reduction of dof, even in capturing the transverse dynamics induced by the geometry that would be dropped in a purely one-dimensional model.

5.5.2 The 3D case

We solve on the 3D domain $\Omega = \Omega_Q \setminus \Omega_L$, with $\Omega_Q = (0,2) \times (0,1) \times (0,2)$ and $\Omega_L = (0,1)^2 \times (1,2)$, the advection-diffusion problem

$$\begin{cases} -\Delta u + \boldsymbol{\beta} \cdot \nabla u = f & \text{in } \Omega \\ u = g & \text{on } \Gamma_{in} \\ \nabla u \cdot \mathbf{n} = 0 & \text{on } \Gamma_{out} \\ u = 0 & \text{on } \Gamma_w, \end{cases}$$

where, for the sake of simplicity, we select a constant field, $\boldsymbol{\beta} = (20, 0, 7)^T$, and with $\Gamma_1 = \{x = 0\} \times (0,1)^2$, $\Gamma_2 = \{x = 2\} \times (0,1) \times (0,2)$, $\Gamma_w = \partial\Omega \setminus \big(\Gamma_{in} \cup \Gamma_{out}\big)$. The forcing term is localized in correspondence with three spherical regions, being $f(x,y,z) = 20\chi_{S_1 \cup S_2 \cup S_3}(x,y,z)$, with $S_1 = \{(x,y,z) \in \Omega : (x-0.7)^2 + (y-0.3)^2 + (z-0.3)^2 \leq 0.1\}$, $S_2 = \{(x,y,z) \in \Omega : (x-1.3)^2 + (y-0.5)^2 + (z-0.5)^2 \leq 0.1\}$, $S_3 = \{(x,y,z) \in \Omega : (x-1.2)^2 + (y-0.6)^2 + (z-1.5)^2 \leq 0.1\}$. Figure 18, left shows the contour plot of the reference 3D linear finite element approximation computed on a structured mesh of uniform sizes, $h_x = h_y = h_z = 1/30$. In particular, the plot refers to the transverse section at $y = 0.5$. It is evident the effect of the Dirichlet data at the inflow, of the field $\boldsymbol{\beta}$ and of the sources, even though the selected section weakly highlights the presence of S_1, while emphasizing the effect of S_2 and S_3.

Concerning the HiMod reduction, we resort to a piecewise hierarchical model reduction applied to the subdomains $\Omega_1 = (0,1)^3$ and $\Omega_2 = (1,2) \times (0,1) \times (0,2)$. The domain decomposition scheme is here employed just as a solver, without selecting a different number of modal functions on Ω_1 and Ω_2. This is partially justified by the complex dynamics of the phenomenon at hand on the whole domain. Moreover, the enforcement of homogeneous Dirichlet data on the entire lateral surface leads us to consider standard sinusoidal functions as modes. A uniform one-dimensional discretization of step size $h = 1/30$ is employed along the supporting fiber Ω_{1D}. We analyze two different configurations, with 100 and 200 modes in both the subdomains, respectively. The relaxed Dirichlet/Neumann scheme converges after a few iterations and provides the approximations in Figure 18, center ($m = 100$) and right ($m = 200$). The HiMod(100) solution is comparable with the reference one in Figure 18, left despite a lack of accuracy can be appreciated along the edge $E = \{x = 1\} \times (0,1) \times \{z = 1\}$. The matching of the two reduced solutions along E is a challenging task. In fact, the modal functions on Ω_1 are identically equal to zero on $(0,1)^2 \times \{z = 1\}$ due to the Dirichlet data, whilst the modes involved in Ω_2 are free to assume any value across $(1,2) \times (0,1) \times \{z = 1\}$. As expected, the mismatch between the two approximations diminishes when we move away from E, since no boundary data constrains the projection of a HiMod basis onto the other one. This effect fades away when considering the finer approximation, HiMod(200).

Finally, to qualitatively assess the performances of the e-HiMod procedure, we modify the boundary data assigned on the faces $F_B = (0,2) \times (0,1) \times \{z =$

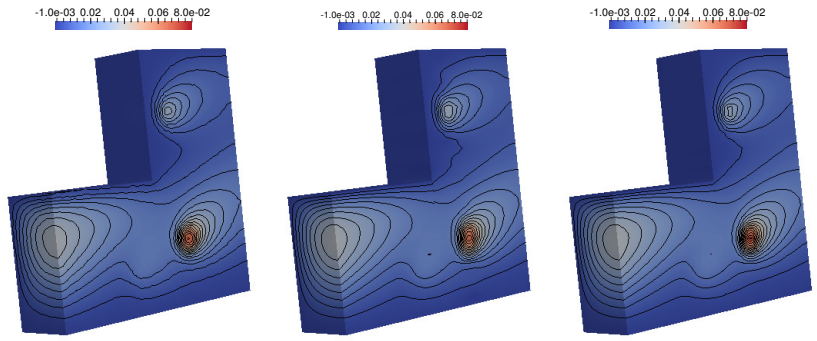

Fig. 18 3D backward facing step, Dirichlet data: reference finite element approximation (left); HiMod(100) (center) and HiMod(200) (right) reduced solutions.

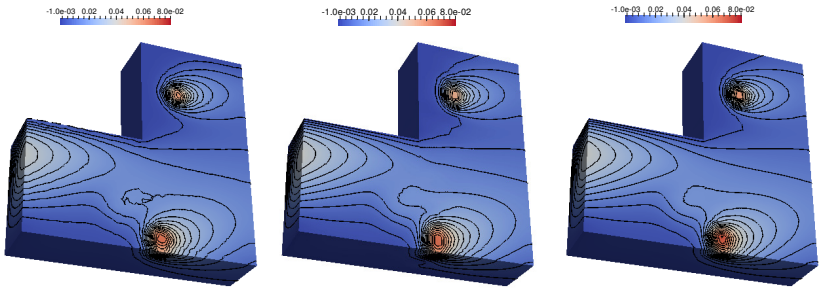

Fig. 19 3D backward facing step, Dirichlet/Robin data: reference finite element approximation (left); e-HiMod(100) (center) and e-HiMod(200) (right) reduced solutions.

0} and $F_T = (1,2) \times (0,1) \times \{z = 2\}$. Here we enforce now the Robin data $\nabla u \cdot \mathbf{n} + 4u = 0$. We also move the location of the sources S_2 and S_3 by centering them at $(1.1, 0.5, 0.1)$ and $(1.3, 0.5, 1.5)$, respectively. The assignment of the Robin condition and the shift, downward, of S_2 yield a complex dynamics in the bottom part of the domain and, in particular, on F_B, as shown by the contour plot of the reference linear finite element approximation in Figure 19, left (transverse section at $y = 0.5$). For the HiMod reduction and the domain decomposition scheme, we preserve the choices previously made except for the use of a modal basis, now educated with respect to the Robin condition. In Figure 19, center and right we show the contour plot of the e-HiMod(100) and e-HiMod(200), respectively. As expected, the accuracy of the reduced solution improves by increasing the number of educated modal functions.

6 Conclusions and perspectives

Despite of its simplicity, several details of the HiMod reduction procedure need to be still addressed. In this paper we have extensively considered the problem of assigning general boundary conditions on the wall of pipes. This is a crucial issue in view of practical applications of HiMod, for instance, to fluid-structure interaction problems, where the effect of the structure on the fluid can be modeled by Robin boundary conditions on the vessel boundaries [4].

We demonstrated that the construction of customized basis functions based on the solution of SLE problems provides an effective approach for automatically incorporating general boundary conditions with the same performances previously obtained for Dirichlet conditions. Results have been rigorously proved, with a view to the SLE approximation theory. We also detected some cases that imply superconvergent results, depending of the type of boundary conditions and of the regularity of the solution. More in general, results in Section 5 are mainly intended to provide a proof of concept of the e-HiMod procedure and to corroborate the proposed theory. We stress again that e-HiMod is not intended to provide a new three-dimensional solver, but to give a method for modulating the accuracy for the secondary transverse dynamics, so to be able of covering networks of pipes by improving simple one-dimensional models. Indeed, the numerical assessment shows that e-HiMod can work on non-trivial geometries, yet approaching the full solution via a "psychologically" one-dimensionally framework. An appropriate selection of the modes m can attain the right trade-off for working on networks. For test cases on real geometries with an extensive comparison of CPU times, we refer to [19, 14].

Following up the contributions mentioned above, we plan to apply the e-HiMod procedure to more complex problems, including the incompressible Navier-Stokes equations in both rectilinear and curved cylindrical pipes, to be applied to simplified models of the human circulation, in the spirit of [19]. Concerning curved geometries, after a first contribution in [23], curved geometries have been considered more recently in [25] - where isogeometric analysis replaces the finite element discretization along the mainstream - and in [19] with a Legendre polynomial approximation of transverse dynamics (called Transversally Enriched Pipe Element Method). It is worth reminding that one-dimensional networks in fluid dynamics are currently the only viable option, for instance, for mathematical modeling of the human circulation over a large number of vessels (see [16] with more than 2000 arteries included). The e-HiMod approach candidates to work out similar problems with more accuracy, possibly adapted to specific regions of interest for the rapid and reliable simulation of blood in the circulation.

Finally, the computational advantages of the one-dimensional coupled pattern of the linear system characterizing the e-HiMod procedure needs to be explored as well. This is expected to further improve the computational advantages of the HiMod methodology.

Acknowledgements The second author acknowledges the support of MIUR-PRIN 2010/2011 project "Innovative Methods for Water Resources under Hydro-Climatic Uncertainty Scenarios" for the financial support. The second and the third authors acknowledge the support of NSF Grant DMS-1419060 "Hierarchical Model Reduction Techniques for Incompressible Fluid-Dynamics and Fluid-Structure Interaction Problems" for this research. The authors wish to thank also Prof. Sandro Salsa for fruitful discussions concerning the analysis of the method, and Pablo J. Blanco for hosting the first author for one month at Laboratório Nacional de Computacao Científica in Petrópolis, Brazil.

References

1. Aletti, M.C.: Educated Basis for Hierarchical Model Reduction in 2D and 3D. Master Thesis, Politecnico di Milano, Italy (a.y. 2012-2013)
2. Aletti, M., Bortolossi, A., Perotto, S., Veneziani, A.: One-dimensional surrogate models for advection-diffusion problems. In: A. Abdulle, S. Deparis, D. Kressner, F. Nobile and M. Picasso, eds., Numerical Mathematics and Advanced Applications, Lect. Notes Comput. Sci. Eng. Vol. **103**, Springer, pp. 447–456 (2015)
3. Azaiez, M., Shen, J., Xu, C., Zhuang, Q.: A Laguerre-Legendre spectral method for the Stokes problem in a semi-infinite channel. SIAM J. Numer. Anal. **47**(1), 271–292 (2009)
4. Badia, S., Nobile, F., Vergara, C.: Fluidstructure partitioned procedures based on Robin transmission conditions. J. Comput. Phys. **227**(14), 7027–7051 (2008)
5. Boyd, J.P.: Chebyshev and Fourier Spectral Methods. Dover Publications, Inc., Mineola, NY (2001)
6. Canuto, C., Hussaini, Y., Quarteroni, A., Zang, T.A.: Spectral Methods: Fundamentals in Single Domains. Springer, Berlin (2006)
7. Canuto, C., Hussaini, Y., Quarteroni, A., Zang, T.A.: Spectral Methods: volution to Complex Geometries and Applications to Fluid Dynamics. Springer, Berlin (2007)
8. Canuto, C., Maday, Y., Quarteroni, A.: Analysis of the combined finite element and Fourier interpolation. Numer. Math. **39**(2), 205–220 (1982)
9. Canuto, C., Maday, Y., Quarteroni, A.: Combined finite element and spectral approximation of the Navier-Stokes equations. Numer. Math. **44**(2), 201–217 (1984)
10. Ern, A., Guermond, J.-L.: Theory and Practice of Finite Elements. Applied Mathematical Sciences **159**, Springer-Verlag, New York (2004)
11. Ern, A., Perotto, S., Veneziani, A.: Hierarchical model reduction for advection-diffusion-reaction problems. In: K. Kunisch, G. Of and O. Steinbach, eds., Numerical Mathematics and Advanced Applications, Springer-Verlag, Berlin Heidelberg, pp. 703–710 (2008)
12. Estrada, E.: The Structure of Complex Networks: Theory and Applications. Oxford University Press (2011)
13. Formaggia, L., Quarteroni, A., Veneziani, A.: Multiscale models for the Vascular System. In: L. Formaggia, A. Quarteroni and A. Veneziani, eds., Cardiovascular Mathematics, Springer, pp. 395-446 (2009)
14. Guzzetti, S., Perotto, S., Veneziani, A.: Hierarchical model reduction in cylindrical domains. In preparation (2016)
15. Landau, L.: Monotonicity and bounds on Bessel functions. Mathematical Physics and Quantum Field Theory, Electronic J. Diff. Eq., Conf. 04, pp. 147–154 (2000)
16. Larrabide, I., Blanco, P.J., Urquiza, S.A., Dari, E.A., Vénere, M.J., Silva de Souza, N.A., Feijóo, R.A.: HeMoLab–Hemodynamics Modelling Laboratory: An application for modelling the human cardiovascular system. Comput. Biol. Med. **42**(10), 993–1004 (2012)
17. `https://cmcsforge.epfl.ch/doxygen/lifev/`.
18. Lions, J.L., Magenes, E.: Non Homogeneous Boundary Value Problems and Applications. Springer, Berlin-Heidelberg-New York (1972)
19. Mansilla Alvarez, L.A., Blanco, P.J., Feijoo, R.A., Bulant, C.A., Dari, E.A., Veneziani, A.: Transversally Enriched Pipe Element Method (TEPEM). An effective numerical approach for blood flow modeling. Accepted for the publication in Int. J. Num. Meth. Biomed. Eng. (2016)

20. Ohlberger, M., Smetana, K.: A dimensional reduction approach based on the application of reduced basis methods in the framework of hierarchical model reduction. SIAM J. Sci. Comput. **36**(2), A714–A736 (2014)
21. Osiadacz, A.: Simulation and Analysis of Gas Networks. Gulf Publishing Company, Houston, TX (1987)
22. Peiró, J., Veneziani, A.: Reduced models for the cardiovascular system. In: L. Formaggia, A. Quarteroni and A. Veneziani, eds., Cardiovascular Mathematics, Springer, pp. 347–394 (2009)
23. Perotto, S.: Hierarchical model (Hi-Mod) reduction in non-rectilinear domains. In: J. Erhel, M. Gander, L. Halpern, G. Pichot, T. Sassi and O. Widlund, eds., Domain Decomposition Methods in Science and Engineering, Lect. Notes Comput. Sci. Eng. Vol. **98**, Springer, Cham, pp. 477–485 (2014)
24. Perotto, S., Ern, A., Veneziani, A.: Hierarchical local model reduction for elliptic problems: a domain decomposition approach. Multiscale Model. Simul. **8**(4), 1102–1127 (2010)
25. Perotto, S., Reali, A., Rusconi, P., Veneziani, A.: HIGAMod: A Hierarchical IsoGeometric Approach for MODel reduction in curved pipes. In press, Comp & Fluids (2016)
26. Perotto, S., Veneziani, A.: Coupled model and grid adaptivity in hierarchical reduction of elliptic problems. J. Sci. Comput. **60**(3), 505–536 (2014)
27. Perotto, S., Zilio, A.: Hierarchical model reduction: three different approaches. In: A. Cangiani, R.L. Davidchack, E. Georgoulis, A.N. Gorban, J. Levesley and M.V. Tretyakov, eds., Numerical Mathematics and Advanced Applications, Springer-Verlag, Berlin Heidelberg, pp. 851–859 (2013)
28. Perotto, S., Zilio, A.: Space-time adaptive hierarchical model reduction for parabolic equations. Adv. Model. and Simul. in Eng. Sci. **2**(25) (2015)
29. Pinchover, Y., Rubinstein, J.: An Introduction to Partial Differential Equations. Cambridge University Press, Cambridge (2005)
30. Quarteroni, A., Veneziani, A., Vergara, C.: Geometric multiscale modeling of the circulatory system between theory and practice. Comput. Methods Appl. Mech. Engrg **302**, 193–252 (2016)
31. Salsa, S.: Partial Differential Equations in Action. Springer, Milan (2015)
32. Vogelius, M., Babuška, I.: On a dimensional reduction method. I. The optimal selection of basis functions. Math. Comp. **37**, 31–46 (1981)
33. Vogelius, M., Babuška, I.: On a dimensional reduction method. II. Some approximation-theoretic results. Math. Comp. **37**, 47–68 (1981)
34. Vogelius, M., Babuška, I.: On a dimensional reduction method. III. A posteriori error estimation and an adaptive approach. Math. Comp. **37**, 361–384 (1981)
35. Zielinski, L.: Asymptotic distribution of eigenvalues for elliptic boundary value problems. Asympt. Anal. **16**(3), 181–201 (1998)